FETPY: a Diiron(I) Thio-Carbyne Complex with Prominent Anticancer Activity in Vitro and in Vivo

Ekatarina Mihajlović,[a] Lorenzo Biancalana,*[b] Sanja Jelača,[a] Lorenzo Chiaverini,[b],# Biljana Dojčinović,[c] Duško Dunđerović,[d] Stefano Zacchini,[e] Sanja Mijatović,[a] Danijela Maksimović-Ivanić,*[a] and Fabio Marchetti*[b]

[a] Department of Immunology, Institute for Biological Research "Siniša Stanković" - National Institute of the Republic of Serbia, University of Belgrade
11108 Belgrade, Serbia
E-mail address: nelamax@ibiss.bg.ac.rs

[b] Department of Chemistry and Industrial Chemistry
University of Pisa
Via Giuseppe Moruzzi 13, I-56124 Pisa, Italy
E-mail addresses: lorenzo.biancalana@unipi.it; fabio.marchetti@unipi.it
#Present address: Department of Pharmacy, University of Pisa, Via Bonanno Pisano 12, I-56126 Pisa, Italy

[c] Institute of Chemistry, Technology and Metallurgy
University of Belgrade,
Njegoševa 12, 11000 Belgrade, Serbia

[d] Institute of Pathology, School of Medicine
University of Belgrade
dr Subotića 1, 11000 Belgrade, Serbia

[e] Department of Industrial Chemistry "Toso Montanari"
University of Bologna
Via P. Gobetti 85, I-40129 Bologna, Italy.

Abstract

FETPY, an organo-diiron(I) complex, showed strong cytotoxicity across a panel of human and mouse cancer cell lines, combined with an outstanding selectivity compared to non-malignant cells. Enhanced iron uptake in aggressive, low-differentiated cell lines, caused membrane lipid peroxidation, which resulted in ferroptosis in human ovarian cancer cells. **FETPY** induced significant morphological changes in murine B16-F1 and B16-F10 melanoma cells, leading to senescence and/or trans-differentiation into Schwann-like cells, thus significantly reducing their tumorigenic potential. Additionally, **FETPY** substantially suppressed tumor growth in low and high-grade syngeneic melanoma models when administered in a therapeutic regimen. **FETPY** is featured by satisfactory water solubility (millimolar range), amphiphilic character (Log P_{ow} = –0.17) and excellent stability in a biological medium (DMEM). These important requisites for drug development are rarely met in iron complexes investigated so far as possible anticancer agents. Overall, **FETPY** holds promise as a safe and potent targeted antitumor agent.

Keywords: anticancer drugs; diiron complexes; carbyne ligand; ferroptosis; in vivo studies

1. Introduction.

Conventional chemotherapy consists of mixtures of drugs that impact growing and dividing cells, leading to their death.[1] A few platinum-based drugs are presently employed in numerous anticancer treatments; however, despite their unquestionable efficacy, they exhibit certain severe limitations, which primarily involve a lack of selectivity, affecting numerous healthy cells and thus resulting in significant adverse effects.[2,3,4] An ultimate goal of the research is to formulate new and effective drugs, preferentially not heavy metal-based, that can overcome the critical challenges associated with platinum compounds.[5,6,7] Iron is a bio essential element that, in various Fe^{II} or Fe^{III} forms, plays a range of functions across vital processes.[8] with some of these functions relying on the interconversion between the two adjacent oxidation states. On the other hand, this versatility can also be a potential source of toxicity, therefore the maintenance of iron homeostasis is closely regulated within healthy cells, primarily through the actions

of iron regulatory proteins (IRP1 and IRP2).[9] Numerous studies highlight that cancer cells, unlike their healthy counterparts, manifest an iron-seeking phenotype: to fulfill the increased iron demand arising from their rapid proliferation, cancer cells need to reconfigure their metabolism to accumulate iron intracellularly - a phenomenon often referred to as "iron addiction".[10] This reconfiguration entails upregulating the expression of transferrin receptor 1 (TfR1), which enhances iron uptake, and concurrently increasing the expression of ferritin, a protein responsible for iron-storage.[11,12,13] Additionally, cancer cells reduce the expression of ferroportin-1, a protein that regulates iron efflux.[14,15] Changes in iron metabolism and the resulting accumulation, in combination with reactive oxygen species (ROS), could promote ferroptosis, which is a form of cell death driven by iron-dependent lipid peroxidation.[16,17,18,19]

In this setting, iron emerges as a privileged element for the advancement of selective anticancer metal drugs.[20] In recent decades, significant efforts have been focused in this area, with the large prevalence of studies regarding iron(II) compounds. In particular, ferrocene derivatives [i.e., mono-iron complexes derived from the ferrocenyl skeleton, $FeCp_2$ (Cp = η^5-C_5H_5), through substitution typically on one Cp ring] have undergone intensive investigation and exhibit a significant potential.[21,22]

Nonetheless, there are certain drawbacks that could complicate progress in this direction. In particular, the typical charge-neutral nature of ferrocenes, conjugated with an extensive hydrophobic structure, may determine substantial lipophilicity and insufficient water solubility. Consequently, ferrocene derivatives might necessitate some form of encapsulation for in vivo studies and, in perspective, for clinical use.[23]

In general, a balanced hydrophilic/lipophilic character (usually measured for metal compounds in terms of octanol/water partition coefficient, Log P_{ow}) is important to facilitate drug internalization in cancer cells[24,25] and, at the same time, avoid systemic toxicity.[26] Furthermore, the peculiar structure of ferrocenes offers limited ligand diversity, considering that the coordination set around the iron center is saturated by the two cyclopentadienyl ligands.

A lesson learned from Nature is that an organo-diiron core can promote cooperativity effects leading to coordination versatility and enabling unique reactivity patterns.[27,28,29] Specifically, [FeFe] hydrogenase

enzymes are found in anaerobic organisms, where they catalyze the reversible oxidation of molecular hydrogen with great efficiency;[30] their active site consists of a diiron unit stabilized by carbonyl and cyanide ligands, and a bridging dithiolate group. The [FeFe] hydrogenase active site is indeed a fascinating and inspiring platform for the construction of diiron carbonyl compounds designed for applications in a physiological environment.[31,32] In this regard, $[Fe_2Cp_2(CO)_4]$ is a commercially available, cost-effective, and convenient starting material to access a remarkable variety of organometallic structures with tunable properties.[33,34,35,36] Notably, cationic complexes with a bridging amino-substituted carbyne ligand (CNR_2^+, R = alkyl/aryl substituent) are straightforwardly obtained from $[Fe_2Cp_2(CO)_4]$. The net positive charge and the robust organometallic assembly prevent oxidation in aqueous solutions, until fragmentation eventually occurs in an intracellular environment.[37,38] The subsequent, presumable release of iron(I) species determines a potent interference with the cellular redox system.[39,40] Note that Fe^I is a nonendogenous oxidation state of iron which has been rarely investigated in medicinal chemistry. Inspired by this concept, in this study we explore for the first time the antitumor potential of three derivatives of $[Fe_2Cp_2(CO)_4]$ comprising a bridging methylthio-substituted carbyne ligand ($CSMe^+$), which shares a structural similarity with the side chain of the amino acid methionine. One complex of the series, possessing optimal prerequisites for drug development (e.g., air stability, appreciable water solubility, amphiphilicity, excellent stability in aqueous environments), emerged for its in vitro performance. Its antitumor activity was assessed in vivo, using syngeneic models of low-invasive and high-invasive mouse melanoma. To the best of our knowledge, examples of iron(I) complexes evaluated in vivo as anticancer drug candidates are missing in the literature, and the same is true for diiron complexes bearing two adjacent iron centers.

2. Results and discussion.

2.1. Synthesis and characterization of diiron complexes

The diiron tris-carbonyl μ-(methylthio)carbyne compound [**1**]CF_3SO_3 was synthesized in two steps from the commercial $[Fe_2Cp_2(CO)_4]$. Although [**1**]CF_3SO_3 and related salts with different anions were

investigated decades ago in pioneering organometallic chemistry under an inert atmosphere,[41,42] we have recently unveiled their suitability for biological applications.[43,44]

The synthesis of [**1**]CF_3SO_3 is described here for the first time. With the aim of varying the coordination set, one CO ligand of [**1**]CF_3SO_3 was replaced with either 4-(dimethylamino)pyridine (DMAP) or 1,3,5-triaza-7-phosphaadamantane (PTA). Note that PTA has been incorporated in several bioactive metal complexes owing to its advantageous physicochemical properties,[45,46] and, notably, some ruthenium(II) arene conjugates (RAPTA complexes) are effective antimetastatic agents pointing to clinical trials.[47] The substitution reactions were successfully carried out in THF solution at reflux temperature, affording [**2**]CF_3SO_3 (**FETPY**) and [**3**]CF_3SO_3, respectively (Scheme 1). Complex [**2**]$^+$, for which we provide an optimized synthesis as triflate salt and comprehensive spectroscopic characterization, was previously isolated as [**2**]PF_6,[48] while [**3**]$^+$ is unprecedented.

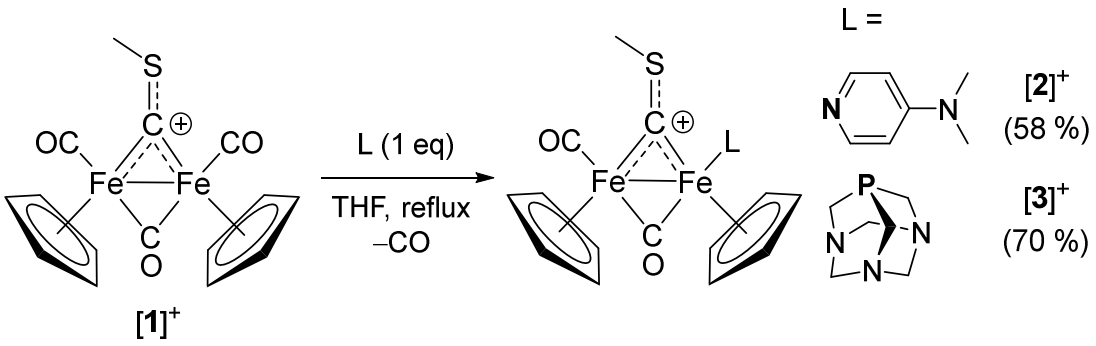

Scheme 1. Synthesis of diiron dicarbonyl μ-(methylthio)carbyne complexes with 4-dimethylaminopyridine (DMAP, [**2**]$^+$) or 1,3,5-triaza-7-phosphaadamantane (PTA, [**3**]$^+$) ligands (donor atom in bold). Triflate ($CF_3SO_3^-$) as counteranion, isolated yields in parentheses.

IR, NMR and ESI-MS spectra of [**1**-**3**]CF_3SO_3 are provided in Figures S1-S13 (Supporting Information). The ^{1}H and ^{13}C NMR spectra of [**1**]CF_3SO_3 (in acetone-d_6) show a single set of resonances (including the diagnostic ^{13}C signal for the thio-carbyne carbon at 408.2 ppm[42,49]), wherein those related to Cp and CO ligands are non-coincident. The lack of C_s symmetry is due to the hindered rotation of the S-methyl group around the μ-C-S bond.[41,50] Likewise, the NMR spectra of [**2**]CF_3SO_3 display a single set of signals, with considerable line broadening for both Cp and S-Me resonances (*e.g.*, the resonance for the S-Me is barely visible in the ^{13}C NMR spectrum, to be compared with the sharp and intense NMe_2 adjacent resonance,

see Figure S6). Instead, the ^{1}H, ^{13}C and ^{31}P NMR spectra of [**3**]CF_3SO_3 display two sets of signals (isomer ratio ≈ 2), indicative of a relatively hampered μ-C-S rotation. ^{1}H NOESY experiments, upon selective irradiation of the cyclopentadienyl resonances, led to identify the *cis* and *cis-E* [51] stereochemistry for [**2**]$^{+}$ and for the major isomer of [**3**]$^{+}$, respectively. The molecular structure of [**3**]$^{+}$ was determined as its [**3**]$CF_3SO_3 \cdot (H_2O)_{2.33}$ salt (Figure 1). The cation is composed of a *cis*-Fe_2Cp_2(μ-CO) core bonded to a bridging methyl-(thio)carbyne ligand, as well as one PTA and one CO ligand both terminally coordinated. Two independent cations are present within the unit cell, both showing disorder of the relative position of the μ-CO and μ-CSMe groups. However, the methyl group lies on the same side of the PTA ligand (*cis-Z* isomer, being the minor isomer in solution, see above). The C(3)-S(1) interaction [1.66(4) Å] displays a considerable π-character consistent with a partial sulfonium nature;[42,52] on the other hand, S(1)-C(4) [1.80(2) Å] is a pure σ-bond. The Fe(1)Fe(2)C(1)C(3) core is almost flat (mean deviation from the least square-plane 0.0917 Å). H-bonds are present in the solid-state structure, involving the H_2O molecules, the N-atoms of PTA and the O-atoms of $CF_3SO_3^{-}$ (Table S1).

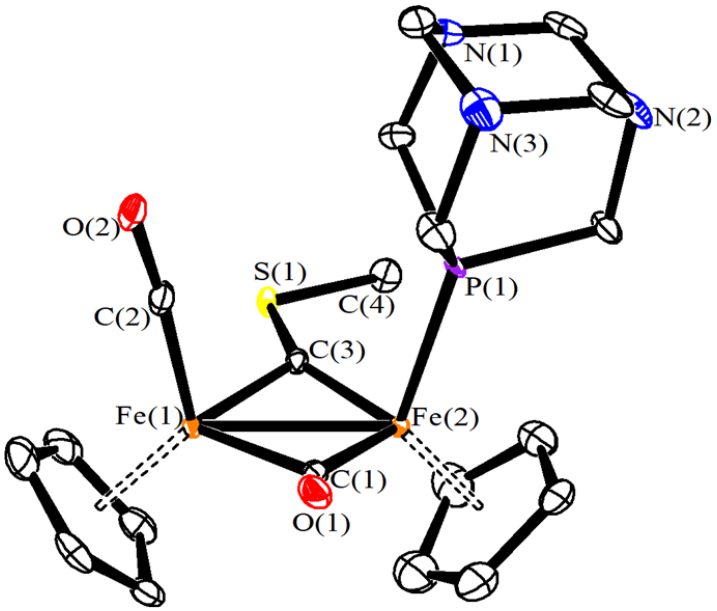

Figure 1. View of the structure of the cation within [**3**]$CF_3SO_3 \cdot (H_2O)_{2.33}$. Displacement ellipsoids are at the 50% probability level. H-atoms have been omitted for clarity. Only the major image of one of the two disordered independent molecules present in the unit cell is represented. Main bond distances (Å) and angles (°): Fe(1)-Fe(2) 2.5016(18), Fe(1)-C(1) 1.96(6), Fe(2)-C(1) 1.86(6), Fe(1)-C(2) 1.745(10), Fe(1)-C(3) 1.93(5), Fe(2)-C(3) 1.76(3), Fe(2)-P(1) 2.204(3), C(1)-O(1) 1.21(7), C(2)-O(2) 1.148(12), C(3)-S(1) 1.66(4), S(1)-C(4) 1.80(2), Fe(1)-C(1)-Fe(2) 82(2), Fe(1)-C(2)-O(2) 175.3(9), Fe(1)-C(3)-Fe(2) 85.3(18), C(3)-S(1)-C(4) 106.4(15). Some care must be taken in evaluating the bonding parameters of the disordered ligands. CCDC reference number 2323915.

2.2. Behavior of the complexes in aqueous solutions

The behavior of [**1-3**]CF_3SO_3 in aqueous media was assessed in terms of D_2O solubility, octanol/water partition coefficient and stability in pseudo-physiological solutions at 37 °C (see Table 1 and ESI for details). Briefly, all compounds are soluble in the millimolar range, with a degree of lipophilicity (Log P_{ow} values) following the order $[\mathbf{2}]^+ > [\mathbf{1}]^+ > [\mathbf{3}]^+$. Notably, the introduction of DMAP or PTA as a ligand in place of one CO (as shown in Scheme 1) imparts high stability to the resulting organo-diiron structures. Thus, [**2-3**]CF_3SO_3 are permanently stable in air and show minimal changes after 24-48 h in the examined solutions (< 10 % degradation in deuterated DMEM cell culture medium). Presumably, the minor aqueous degradation of [**1-3**]CF_3SO_3 occurs with extensive fragmentation of the diiron core, including the elimination of carbon monoxide, which was quantified (approximately 2 eq. per degraded complex, see Table 1). Remarkably, the controlled CO release in a cancer environment has been promisingly investigated as a pharmacological strategy.[53,54]

Table 1. Behavior of diiron complexes in aqueous solutions (see ESI for details). Solubility in water (D_2O) and octanol/water partition coefficient (Log P_{ow}) at 21 °C. Residual starting material and equivalents of carbon monoxide released after 24-48 h at 37 °C in water or in cell culture medium solution (or their mixtures with methanol)

Comp.[a]	D_2O solubility (mol/L)	Log P_{ow}	% Residual complex [b]		Eq. CO [c]
			37 °C, 48 h D_2O±CD_3OD	37 °C, 24 h DMEM±CD_3OD	37 °C, 24 h H_2O±MeOH
[**1**]CF_3SO_3	$8.5\cdot10^{-3}$	−0.70 ± 0.05	65	64	0.66
[**2**]CF_3SO_3	$6.3\cdot10^{-4}$	−0.17 ± 0.05	91	93	0.17
[**3**]CF_3SO_3	$5.3\cdot10^{-3}$	< −1.5	87	91	0.15

[a] All compounds as $CF_3SO_3^-$ salts. Results are referred collectively to all isomers present in the solution. For each compound, stability experiments were carried out in 100 % aqueous solution ([**1**]$^+$, [**3**]$^+$) or a in water/methanol 3/2 *V*/*V* mixture ([**2**]$^+$). [b] Calculated by ^{1}H NMR with respect to the initial spectrum (Me_2SO_2 as internal standard). [c] Released carbon monoxide, determined by GC-TCD analysis (relative standard deviation below 15 %), reported as the molar ratio with respect to the starting complex (n_{CO}/n_{Fe2}).

2.3. In vitro antiproliferative activity of diiron thio-carbyne complexes

Complexes [**1-3**]CF_3SO_3 were tested on three human cancer cell lines with different origins and invasive potentials (HCT 116, MCF7, and A2780). Specifically, alterations in iron metabolism and the maintenance of homeostasis in cancer cells are closely associated with the acquisition of an aggressive phenotype. Although malignant cells differ in their characteristics depending on the tissue from which they originate, in malignant transformation they undergo a process of dedifferentiation during which they acquire a stem phenotype associated with altered iron requirements. A2780 and HCT 116 cells represent advanced tumor stage falling into the above-mentioned range. On the other hand, MCF7 is a hormone-positive, i.e. less aggressive, breast cancer cell line whose iron metabolism is rapidly impaired by the acquisition of a chemotherapy-resistant phenotype. To outline a possible selectivity, human fetal lung fibroblasts (MRC5) were included in the present study.

The IC_{50} values obtained with the examined complexes are compiled in Table 2 (see also Figure S14), along those related to cisplatin under identical experimental conditions for comparison.

Table 2. IC_{50} values (μM) ± standard deviation of diiron complexes and cisplatin[55] on human cell lines determined after 72 hours of treatment using MTT and CV viability assays.

Cell line	Viability assay	[**1**]CF_3SO_3	[**2**]CF_3SO_3	[**3**]CF_3SO_3	Cisplatin [55]
HCT 116 Colorectal carcinoma	MTT	>200	4 ± 0.1	>200	1.5 ± 0.1
	CV	>200	12 ± 0.9	>200	8.0 ± 0.7
MCF7 Breast cancer	MTT	88.3 ± 2.3	2.1 ± 0.2	>200	0.8 ± 0.2
	CV	124.5 ± 7.6	5.1 ± 0.4	>200	1.2 ± 0.3
A2780 Ovarian cancer	MTT	45.8 ± 1.8	2.5 ± 0.2	155 ± 8.5	1.9 ± 0.2
	CV	58.6 ± 3.6	4.9 ± 0.2	135.5 ± 4.4	3.8 ± 0.5
MRC5 Lung fibroblasts	MTT	>200	58 ± 5.2	>200	0.6 ± 0.2
	CV	>200	81 ± 4.2	>200	0.8 ± 0.1

Among the examined diiron complexes, the viability tests reveal the superior cytotoxic potential of [**2**]CF_3SO_3, which IC_{50} values related to cancer cells are slightly higher than those detected upon treatment with cisplatin. Importantly, a marked preference of [**2**]CF_3SO_3 for cancer cell lines is evident, highlighting

the strong affinity of this complex towards the malignant phenotype. This selectivity becomes prominent when comparing the IC_{50} values for MRC5 vs. A2780 cell lines (average ratio ≈ 20). It should be mentioned that the triflate anion ($CF_3SO_3^-$) was previously associated with various cationic metal complexes, and some of the resulting salts did not show any appreciable toxicity in vivo and/or in vitro.[56,57] Therefore, it can be inferred that the cytotoxicity of the investigated diiron complexes is ascribable to the specific cationic component. Based on the preliminary results concerning [**1-3**]CF_3SO_3, [**2**]CF_3SO_3 (**FETPY**) was selected for further studies.

2.4. Cellular iron uptake and mechanistic insights

The iron internalization in A2780 cells was measured using ICP-OES. Beyond the observed selectivity, we recognized a striking capability of the cancer cells to acquire iron from **FETPY**. In fact, a time-dependent increase in iron uptake was detected upon incubation of A2780 cells with the IC_{50} dose of **FETPY**: after 24 h, the iron content reached a six-fold higher level than in untreated A2780 cells (Figure 2A). Conversely, no significant variation in intracellular iron concentration was measured in normal cells (MRC5) treated with the same dose of **FETPY** over the same time interval.

The reduced viability of A2780 cells after treatment with IC_{50} dose of **FETPY** is ascribable to inhibited cell division, rather than apoptotic or autophagic cell death. This conclusion is based on CFSE staining, Ann/PI staining, caspase activity, fluorescent microscopy and AO staining (Figure S15). The altered cell morphology was found to be associated with significant membrane lipid peroxidation (C11 BODIPY 581/591 staining) (Figure 2B-C). The addition of ferrostatin-1 (Fer-1) almost completely neutralized this effect, suggesting that **FETPY** induced ferroptosis in A2780 cells (Figure 2B).[58]

Using specific redox-sensitive fluorescent probes (DHR 123, DHE, and DAF-FM), suppressed hydrogen peroxide (H_2O_2) and peroxynitrite ($O{=}NOO^-$), along with amplified production of superoxide anion (O_2^-) and nitric oxide (NO), were recognized in comparison to untreated cells, upon 48h treatment of A2780 cells with **FETPY** (Figure 2D). The notable intracellular redox activity of **FETPY** could be related to the release of iron(I) species, which are subsequently oxidized (based on the common stability of Fe^{3+} in

oxygenated aqueous media) and interfere with cellular O_2 metabolism. On the other hand, the anticancer activity of DMAP was previously recognized,[59,60] and it is possible that its intracellular release, favoured by protonation at physiological pH ($DMAPH^+$: pK_a = 9.6 in water[61]), contributes to the cytotoxicity of **FETPY**.

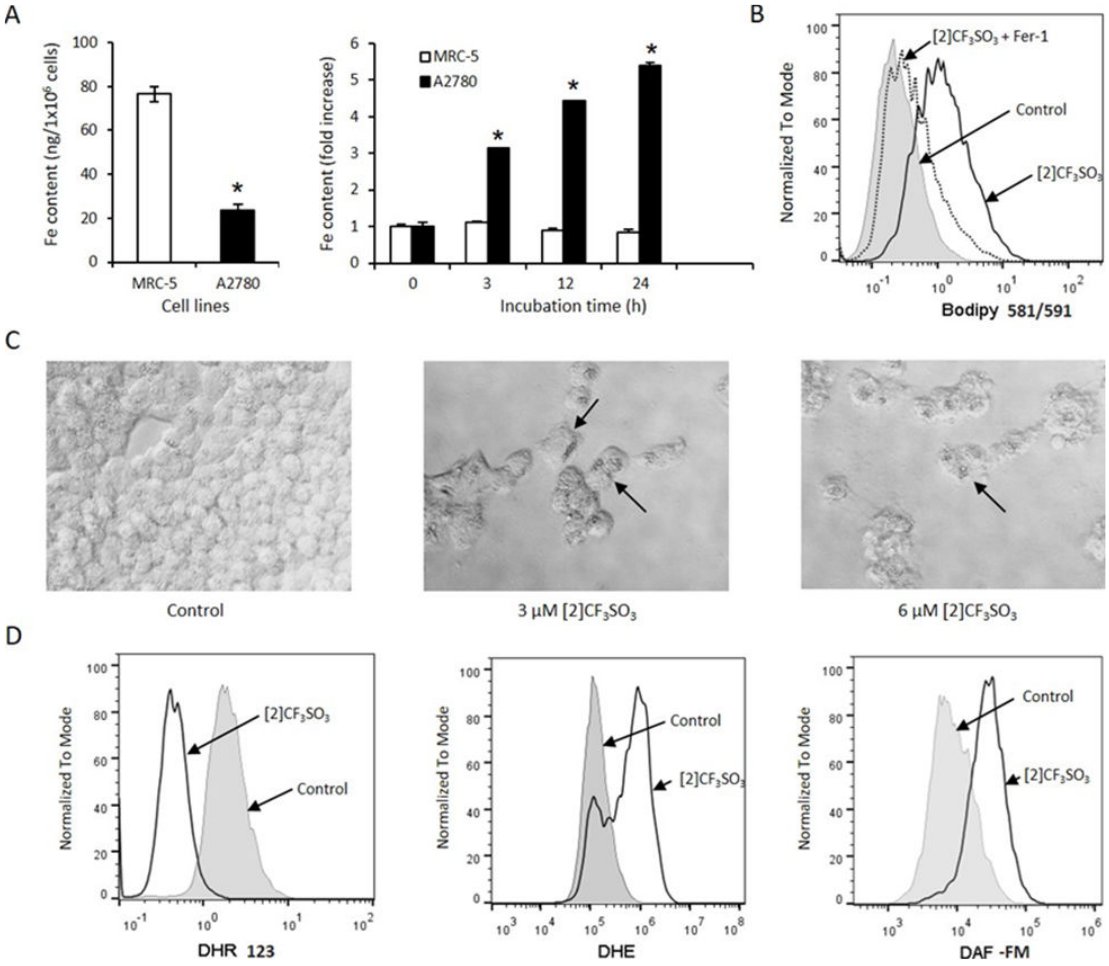

Figure 2. A) Iron content in A2780 and MRC5 cells determined by ICP-OES after 3, 12 and 24 h of treatment with [**2**]CF_3SO_3 (**FETPY**) (* $p < 0.05$ in comparison to MRC5 samples in respective time points); B) Ferroptosis of A2780 cells detected by flow cytometry after 48 h treatment with [**2**]CF_3SO_3; C) Light microscopy of A2780 cells after treatment with [**2**]CF_3SO_3; D) Intracellular levels of reactive oxygen and nitrogen species and nitric oxide in A2780 cells detected by flow cytometry after 48 h treatment with [**2**]CF_3SO_3 (DHR123- hydrogen peroxide and peroxynitrite, DHE- superoxide anion, DAF-FM- nitric oxide).

We note that ferroptosis can be triggered and executed through various forms of iron-dependent lipid peroxidation and there is no linear dependence between the ROS/RNS network and such specific mode

of cell death.[62] However, the correlation between the overproduction of O_2^- and drug-induced ferroptosis was previously documented.[63,64] While it is generally believed that H_2O_2 plays a key role in membrane lipid peroxidation and that NO inhibits this process,[65] our study evidences a specific H_2O_2/O_2^- pattern, suggesting that the presence of O_2^- in conditions of H_2O_2 deficiency is a prerequisite for the **FETPY**-induced ferroptosis in A2780 cells.

2.5. Experiments on murine cell lines

To clarify whether the observed effect provided by **FETPY** is specific to ovarian cancer, as a prototype of the iron-addictive phenotype, or universal across different grades of neoplasia, as well as to pursue the possibility of translating studies to in vivo, we conducted experiments on a range of mouse cell lines. These included low and high-grade melanomas (B16-F1 and B16-F10) and highly aggressive breast triple-negative cancer (4T1) (Figure S16, Table S2). Hence, melanoma cells displayed the highest sensitivity among the tested cell lines, similar to that observed in the human cancer cell line A2780 (Figure S16, Table S3). The selectivity index calculated with respect to NIH-3T3 mouse fibroblasts is around 8. Measurement of intracellular iron content in nontreated cells showed inverse correlation between its quantity and the aggressiveness of malignant cells (Figure 3A left). Accordingly, iron-deficient mouse B16-F10 cells, as well as less aggressive B16-F1 clone, take up more iron during treatment with **FETPY** (5 μM) compared to normal cells (Figure 3B). B16-F10 cells isolated from melanoma lung metastasis exhibited a comparable pattern of iron uptake with respect to that detected in A2780 cells (six-fold increase of iron concentration) after exposure to **FETPY**. On the other hand, the uptake capacity of B16-F1 after treatment with the same dose of **FETPY** was significantly less and only slightly enhanced when compared to NIH 3T3 normal fibroblasts (Figure 3A). Interestingly, incubation of murine melanoma cancer cells with **FETPY** led to evident changes in cell morphology after 72 h. More precisely, B16-F1 cells finally showed a fibroblast-like elongated shape, while B16-F10 cells acquired a neuronal-like phenotype with enlarged cell bodies and long dendritic extensions (Figure 3B). Unlike the response observed in A2780 cells, flow cytometric analysis of membrane lipid peroxidation in both B16 clones

upon exposure to **FETPY** was not reversed by Fer-1. This fact indicates that ferroptosis is not directly correlated with the decreased cell viability triggered by the present treatment (Figure 3C).

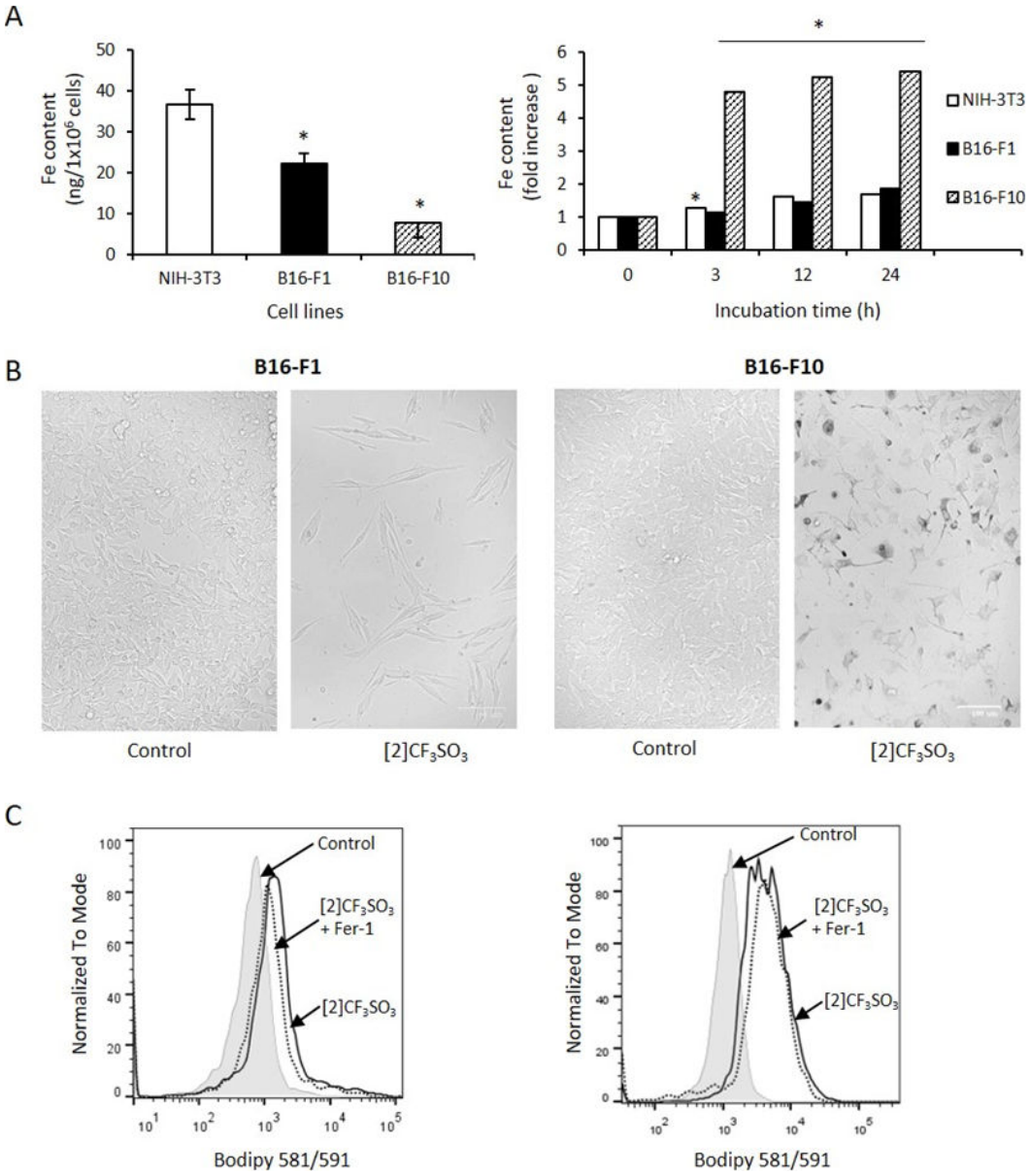

Figure 3. A) Intrinsic iron content in nontreated B16-F1, B16-F10 and NIH-3T3 cells determined by ICP-OES (left) and after 3, 12 and 24 h of treatment with [**2**]CF_3SO_3 (right) (**FETPY**; * $p < 0.05$ in comparison to NIH-3T3 samples in respective time points). B) Light microscopy of B16-F1 and B16-F10 cells after 72 h of treatment with [**2**]CF_3SO_3. C) Detection of ferroptosis by flow cytometry in B16-F1 (left side) and B16-F10 (right side) cells after 72 h treatment with [**2**]CF_3SO_3.

In agreement with what was detected on human ovarian cancer cells, apoptotic/autophagic cell death is not the predominant mode of action of **FETPY** in murine melanoma cell line (Figure S17). Instead, PI staining revealed an increase in cellular nuclear size with a specific texture of chromatin distribution,

resembling cell senescence (Figure S17-C). This senescence-like state was further confirmed by oil-red staining, which visualized the presence of numerous lipid/lipofuscin droplets (Figure 4A).

In conclusion, the mechanism of action of **FETPY** is cell-specific, including ferroptosis in human ovarian cancer cells and senescence in murine melanoma cell lines. Notably, all these effects were more pronounced in the advanced form of melanoma (B16-F10 rather than B16-F1).

The determination of the phenotype of both melanoma cell lines pointed out that the observed morphological change was not accompanied by enhanced expression of melanocytic markers, tyrosinase activity and melanin content, indicating that cells were not subjected to melanocytic differentiation (Figure S18).[66] On the other hand, an intensified expression of myelin basic protein was detected in B16-F10 cells, suggesting the acquisition of Schwann-like phenotype (Figure 4B). The existence of this phenotype is noted as part of trans-differentiation and terminal involution of senescent melanoma cells.[67,68,69]

When cells altered by the in vitro treatment with **FETPY** were inoculated into healthy C57BL6 mice, a significant reduction in tumor-forming potential was observed in comparison to the group of animals inoculated with untreated cells (Figure 4C). As a matter of fact, the tumor volume at the time of sacrifice (day 21) was reduced by 57% and 44% in the B16-F1 and B16-F10 models, respectively, in comparison to the relevant control.

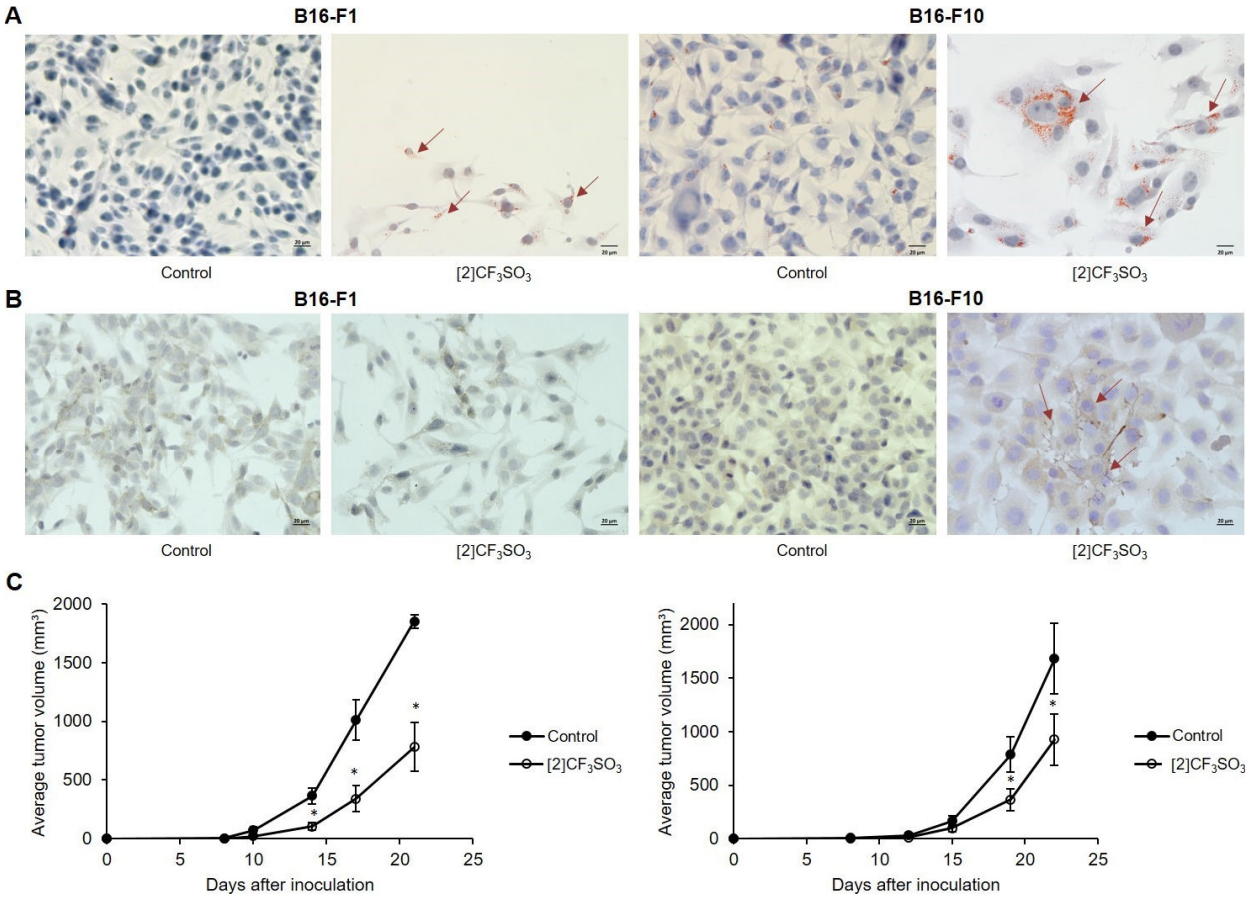

Figure 4. A) Oil red staining of B16-F1 and B16-F10 cells after 72 h of treatment with [**2**]CF_3SO_3 (**FETPY**); B) Immunocytochemistry analysis of B16-F1 and B16-F10 cells stained with MBP antibody after 72 h of treatment with [2]CF_3SO_3; C) Tumor growth curves after inoculation of *in vitro* treated B16-F1 (left side) and B16-F10 (right side) cells with [**2**]CF_3SO_3 (* $p < 0.05$ in comparison to control group which received untreated cells.

Since the redox status of low invasive B16-F1 supports the absence of ferroptosis, its aggressive counterpart (B16-F10) showed production of superoxide and nitric oxide comparable to data on human A2780 cancer cells (Figures 2D and S17). Conversely, DHR 123 staining of B16-F10 cells showed a slight enhancement of hydrogen peroxide and peroxynitrite production, which might be related to a different outcome of treatment and absence of ferroptotic cell death (Figure S19).

Specific inhibition by apocynin of the nicotinamide adenine dinucleotide phosphate (NADPH) oxidase 2 (NOX2), an enzyme responsible for O_2^- production, partly recovered cell viability. This evidence confirms the involvement of NOX2 in the drug-mediated antitumor effect (Figure S19-D). Unlike melanocytes, NOX2 is highly expressed in melanoma cells, leading to autocrine ROS production which

is closely connected with melanogenesis and lipid peroxidation.[70,71] It is conceivable that this enzyme is also involved in the drug-induced melanoma reprogram.

2.6. In vivo studies

Considering that cell culture represents an isolated system and does not fully reflect the heterogeneity and complexity of events defining the outcome of the tumor treatment, the effectiveness of **FETPY** was further evaluated in a syngeneic model of both low (B16-F1) and highly invasive (B16-F10) solid subcutaneous melanoma induced in C57BL/6 mice. The drug was applied in a therapeutic regime, starting when tumors became palpable. As seen in Figure 5A, growth rate and tumor volume were significantly reduced by the treatment with **FETPY** in both models (approximately 75% reduction of final tumor volume in low invasive melanoma and 50% reduction of final tumor volume in highly invasive melanoma, compared to the respective untreated groups).

Histopathological assessment of tumor tissue in the B16-F1 model showed a similar extent of tumor necrosis, as well as moderate presence of pigment across tumor tissue, in both control and treated groups (Figure 5B). However, in tumors isolated from animals treated with **FETPY**, larger areas of cells with swelled empty appearing cytoplasm and pyknotic nuclei, as a possible sign of threatening cell death and reason for necrosis, were noticed. Conversely, within B16-F10 tumor tissue, aside from substantial necrotic areas observable in both groups, the treated group exhibited areas of apoptosis and focal points of tumor cell differentiation in the form of cellular spindling and the production of melanin pigment. These findings suggest that apoptosis and cell differentiation may contribute to the mechanism of drug action. On the other hand, cells in the control group exhibited a more epithelioid morphology, greater cellular pleomorphism, and distinct macronucleoli (Figure 5B).

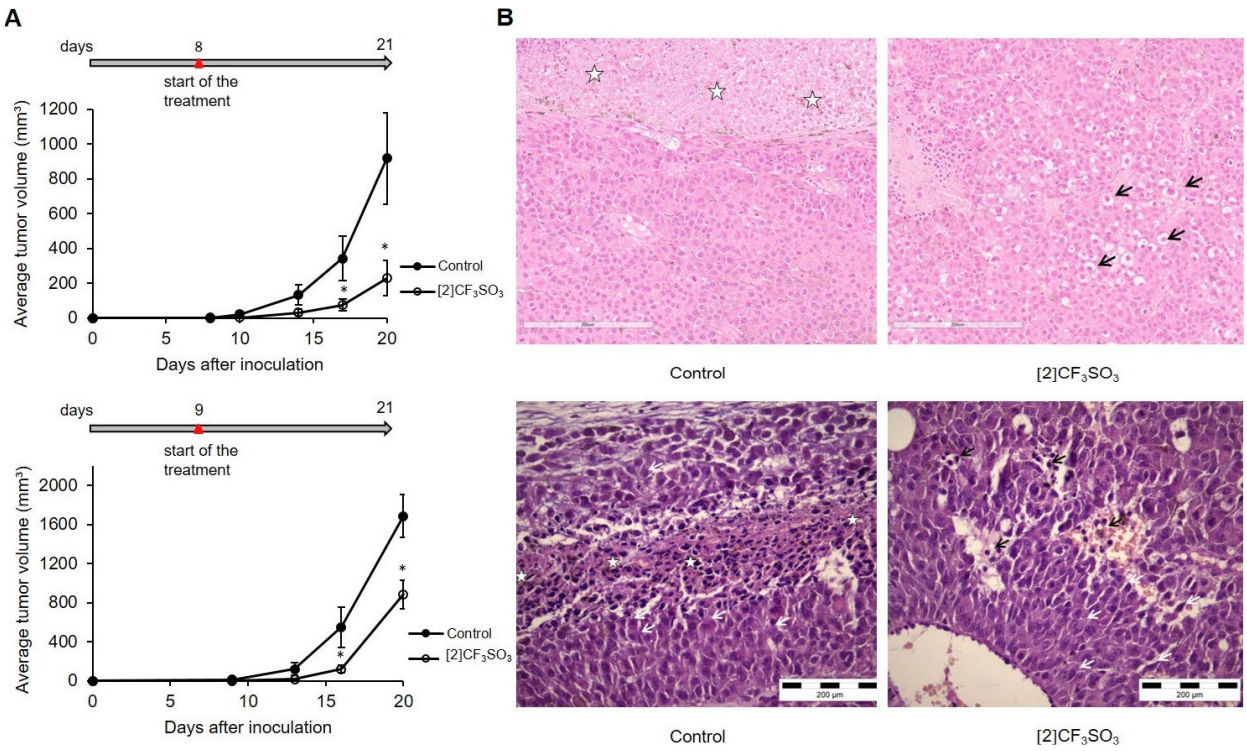

Figure 5. A) Tumor growth curves after inoculation of B16-F1 (upper panel) and B16-F10 (lower panel) cells in C57BL/6 mice. Treatment of animals started when tumors became palpable. The dose regimen was 4mg/kg of [**2**]CF_3SO_3 (**FETPY**) every day until the end of the experiment (* $p < 0.05$ in comparison to control group which received only solvent); B) Hematoxylin-eosin staining of sections of B16-F1 (upper panel) and B16-F10 (lower panel) tumors isolated on the last day of experiment (white stars-areas of tumor necrosis and more epithelioid morphology of malignant melanocytes; white arrows-more differentiated cells with spindling and with some discrete cellular processes; black arrows-areas of apoptosis of tumor cells)

Considering that, in low-grade tumors, the induction of cell death represents the desirable way of tumor cell elimination, while in advanced stages it might trigger tumor repopulation, it appears that $[\mathbf{2}]^+$ exerts its antitumor activity in an optimal way. Remarkably, animals subjected to treatment, concerning both tumor models, showed no visible signs of toxicity. Their behavior, reactions to stimuli, and hygiene habits remained indistinguishable from the control group. Moreover, we did not collect any evidence of eating or drinking disorders, neurological deficits, or alterations in external appearance. Consistently, there were no significant changes in body weight (Figure 6).

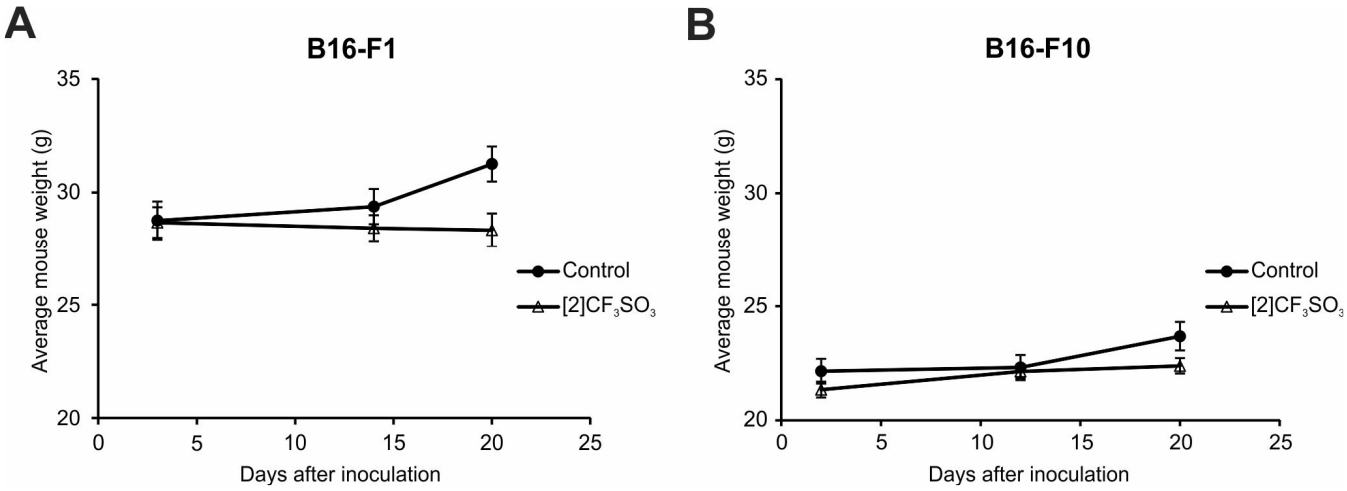

Figure 6. Change in mice weight followed during *in vivo* experiments on low-invasive (A) and high-invasive (B) melanoma model. The data is expressed as average mouse weight per group ± SD at three different time points during the experiment.

Animals were euthanized at day 21 and liver and kidney tissues obtained from both the control and treated group underwent comprehensive microscopic analysis to assess potential indications of toxicity. In the kidney tissues of both groups, no significant alterations or differences in morphology were detected. The tissue architecture, as well as cellular morphology, remained unaffected in both groups. Only a limited number of perivascular mononuclear inflammatory infiltrates, and protein cast within a few convoluted tubules, were detected in both groups (Figure 7A). However, signs of portal chronic hepatitis were observed within the B16-F10 model, marked by an elevated proliferation of biliary ductulus and the presence of lymphocytic infiltrates. Localized regions of small oligocellular and occasionally confluent hepatocyte necrosis were also identified. No other noticeable changes were observed in either group (Figure 7B). On the other hand, in the low-grade B16-F1 model, hepatotoxicity was considerably less pronounced. In the livers of animals treated with **FETPY**, hepatocyte vacuolization was detected (Figure 7B). Biochemical analysis of urine parameters (red blood cells, bilirubin, urobilinogen, ketones, proteins, nitrites, glucose, specific gravity, pH and leukocytes) revealed no difference between control and treated groups of animals, indicating that both the kidneys and the liver preserved their functionality (data not shown).

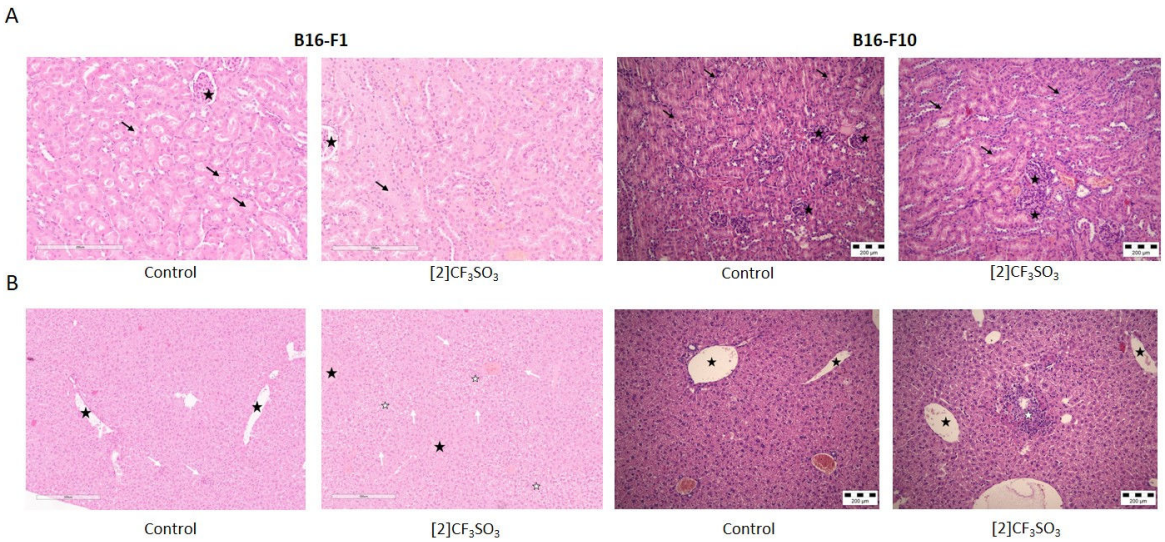

Figure 7. Hematoxylin-eosin staining of the kidney (A) and liver (B) sections isolated at the end of in vivo experiment (Kidney tissue: black arrows- tubules with protein casts; black stars-glomeruli; Liver tissue: white arrows-demarcation of vacuolized hepatocytes from surrounding tissue; white stars-hepatocyte swelling; black stars-portal triads).

3. Conclusions

Iron(II) complexes have been intensively investigated with the aim of developing efficient anticancer drugs that can overcome the serious limitations associated with the platinum complexes currently employed in cancer chemotherapy. However, suitable candidates, combining a promising antitumor activity with important features required for clinical progression, such as sufficient water solubility and balanced hydrophilic/lipophilic character, remain elusive. In this study, we report a prototypal example of an iron(I) compound investigated on *in vivo* models as an anticancer drug candidate. Three diiron carbonyl complexes with a bridging thio-carbyne ligand were synthesized, and that featuring a 4-(dimethylamino)pyridine ligand (**FETPY**) showcased remarkable potential across a range of human and mouse cell lines extracted from tumors with varying origins and levels of aggressiveness. Furthermore, **FETPY** exhibited outstanding selectivity towards cancer cells compared to normal cells. Highly aggressive tumor cell lines displayed enhanced iron uptake capacity. The iron uptake pattern related to **FETPY** varies depending on the intrinsic iron content, metabolic characteristics, and redox response of the tumor cells. The mechanism of action of **FETPY** appears to exhibit cell type-dependent variability: it ranges from induction of ferroptosis, as observed in A2780 cells, to elicitation of senescence and trans-differentiation in melanomas B16-F1 and B16-F10. The tumorigenic potential of these altered cells was drastically reduced upon application in a syngeneic mouse model. When applied in vivo under therapeutic conditions, **FETPY** led to a substantial reduction of tumor volume and animals subjected to treatment in both tumor models showed no visible signs of toxicity. Since inducing cell death in high-grade tumor treatment may be counterproductive and cause tumor repopulation, the observed differentiation of melanomas triggered by **FETPY** might be of special importance.

4. Experimental

4.1. General Details

$[Fe_2Cp_2(CO)_4]$ (99%) was purchased from Strem Chemicals, other reactants and solvents were obtained from Alfa Aesar, Merck or TCI Chemicals and used as received. Methyl triflate and thiophosgene ($CSCl_2$) were stored under N_2 at 4 °C; contaminated labware was treated with NaOH/EtOH. Compound $[Fe_2Cp_2(CO)_2(\mu\text{-}CO)(\mu\text{-}CS)]$ was prepared from $[Fe_2Cp_2(CO)_4]$/Na/$(PhO)_2CS$ according to published procedures[72,73,74] and immediately used for the synthesis of [**1**]CF_3SO_3. All the preparations were carried out under dry N_2 using standard Schlenk techniques. Compounds $(PhO)_2CS$, $[Fe_2Cp_2(CO)_2(\mu\text{-}CO)(\mu\text{-}CS)]$ and [**1-2**]CF_3SO_3 were prepared using anhydrous solvents (THF, CH_2Cl_2 and MeCN distilled from CaH_2 and – except THF – stored over 4 Å MS), while [**3**]CF_3SO_3 was prepared using deaerated BHT-stabilized THF. The reactions were monitored by IR spectroscopy. Neutral alumina (dry, Merck) or silica gel (120 mesh, Merck) were used for column chromatography. The chromatographic purification of $[Fe_2Cp_2(CO)_2(\mu\text{-}CO)(\mu\text{-}CS)]$ and [**1**]CF_3SO_3 was carried out under a N_2 atmosphere using anhydrous solvents. All the other operations, including work-up procedures of [**2**,**3**]CF_3SO_3, were carried out under air with common laboratory glassware. Reaction yields are referred to the isolated, powdered materials. Purity of compounds was checked by elemental analysis and is > 95%. Compounds [**2**-**3**]CF_3SO_3 are air- and moisture- stable in the solid state for months but were stored under N_2 for longer periods of time. Compounds $[Fe_2Cp_2(CO)_2(\mu\text{-}CO)(\mu\text{-}CS)]$ and [**1**]CF_3SO_3 were always stored under N_2 to prevent a slow aerobic oxidation process. NMR spectra were recorded at ambient temperature on a Bruker Avance II DRX400 or JEOL YH JNM-ECZ400S instruments equipped with broadband probes. Chemical shifts (ppm) are referenced to the residual solvent peaks (^1H, ^{13}C) or to external standards (^{19}F to $CFCl_3$, ^{31}P to 85% H_3PO_4).[75,76] ^1H and ^{13}C spectra were assigned with the support of ^1H NOESY (mix time 750 ms, relaxation time 1 sec, linewidth 25 Hz) ^1H-^1H COSY and ^1H-^{13}C *gs*-HSQC experiments. Signals due to the minor isomeric form of [**3**]$^+$ are italicized and the cyclopentadienyl ligand on the same side of the *P*-donor ligand is labelled as Cp^P. $CDCl_3$ stored in

the dark over Na_2CO_3 was used for NMR analysis. IR spectra of solid samples (650-4000 cm^{-1}) were recorded on a Perkin Elmer Spectrum One FT-IR spectrometer equipped with a UATR sampling accessory (ZnSe crystal). IR spectra of solutions were recorded using a CaF_2 liquid transmission cell (1500-2300 cm^{-1}) on a Perkin Elmer Spectrum 100 FT-IR spectrometer. UV-Vis spectra (250-800 nm) were recorded on a Ultraspec 2100 Pro spectrophotometer using PMMA cuvettes (1 cm path length). IR and UV-Vis spectra were processed with Spectragryph.[77] CHNS analyses were performed on a Vario MICRO cube instrument (Elementar). GC analysis was performed on a Clarus 500 instrument (PerkinElmer) equipped with a 5 Å MS packed column (Supelco) and a TCD detector. Samples were analyzed by isothermal runs (110 °C, 4 min) using He as carrier gas. ESI-Q/ToF flow injection analyses (FIA) were carried out using a 1200 Infinity HPLC, coupled to a Jet Stream ESI interface with a Quadrupole-Time of Flight tandem mass spectrometer 6530 Infinity Q-TOF (Agilent). HPLC-MS grade acetonitrile was used as mobile phase. The flow rate was 0.2 mL/min (total run time 3 min). Samples were weighted, dissolved in HPLC-MS grade methanol and diluted to 10 ppm prior to injection. Injection volume: 0.1 μL. ESI operating conditions: drying gas (N_2, purity >98%): 350 °C and 10 L/min; capillary voltage 4.5 KV; nozzle voltage: 1 KV; nebulizer gas 35 psig; sheath gas (N_2, purity >98%): 375 °C and 11 L/min. The fragmentor was kept at 50 V, the skimmer at 65 V and the OCT 1 RF at 750 V. High resolution MS spectra were achieved in positive mode in the range 100-1700 *m*/*z*; the mass axis was calibrated using the Agilent tuning mix HP0321 (Agilent Technologies) prepared in acetonitrile and water.

4.2. Synthesis and Characterization

Diphenyl thiocarbonate (carbonothioic acid, *O*,*O*-diphenyl ester) ($(PhO)_2CS$, Chart 1)

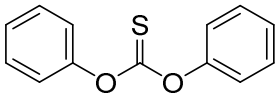

Chart 1. Structure of $(PhO)_2CS$.

The title compound was previously obtained from $PhOH/CSCl_2/Et_3N$ (or related reactants) and isolated following an aqueous work-up.[78,79,80] A novel synthetic procedure, avoiding the use of water, is herein described. In a 500 mL two-necked round-bottom flask under N_2, NaH (dry/90 %, 4.74 g, *ca.* 175 mmol) and THF (120 mL) were introduced. Next, a solution of phenol (20 g, 212 mmol) in THF (60 mL) was slowly added to the mixture under magnetic stirring via a dropping funnel. Therefore, a solution of $CSCl_2$ (11.5 mL, 150 mmol) in THF (30 mL) was added dropwise over 45 min under stirring. Upon addition of the last drops, the mixture turned light yellow and denser due to NaCl precipitation. The mixture was refluxed for 1 hour and then allowed to cool to room temperature. Afterwards, the suspension was filtered using filter paper and the filtrate was dried under vacuum, affording a yellow solid. The residue was triturated following prolonged soaking with pentane (200 mL). The suspension was filtered and a first fraction of the title compound was collected (light yellow powder). The filtrate was stored for a few hours at – 20 °C and the resulting light-yellow crystals were collected (second fraction of the title compound). The solution was separated, reduced to a small volume under reduced pressure and moved on top of a silica column. Impurities were eluted with pentane, then a pale-yellow band was eluted with petroleum ether/Et_2O 8:1 *V*/*V*. Volatiles were removed under vacuum, affording a third crop of the title compound as a light-yellow powder. Overall yield: 26.14 g, 77 % (vs. thiophosgene). Anal. calcd. for $C_{13}H_{10}O_2S$: C, 67.80; H, 4.38; S, 13.92. Found: C, 67.67; H, 4.41; S, 13.90. IR (solid state): $\tilde{\upsilon}/cm^{-1}$ = 3066w, 3051w, 3039w, 1591m, 1488m, 1457w, 1347w, 1338w, 1311w, 1282m-sh, 1259s-sh, 1244s, 1230s (C=S), 1190s-sh, 1152m, 1070m, 1019m, 1002m, 931m, 909w, 795w, 768s, 708s, 687s. ^1H NMR ($CDCl_3$): δ/ppm =

7.50 (t, $^{3}J_{HH}$ = 7.6 Hz, 1H), 7.36 (t, $^{3}J_{HH}$ = 7.3 Hz, 1H), 7.30–7.23 (m, 2H) (Ph). $^{13}C\{^{1}H\}$ NMR ($CDCl_3$): δ/ppm = 195.0 (CS); 153.7, 129.8, 127.0, 122.0 (Ph).

$[Fe_2Cp_2(CO)_2(\mu\text{-}CO)(\mu\text{-}CSMe)]CF_3SO_3$ ([1]CF_3SO_3, Chart 2).

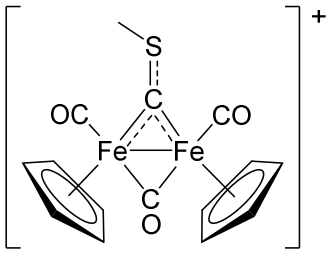

Chart 2. Structure of [**1**]$^{+}$.

The synthetic procedure of the title compound is unprecedented in the literature.[81] The preparation of related BF_4^-, SO_3F^-, I^- and PF_6^- derivatives (22 % overall yield for [**1**]I with respect to $[Fe_2Cp_2(CO)_4]$), together with IR (CH_2Cl_2), ^{1}H NMR (acetone-d_6) and ^{13}C NMR (CD_3CN) characterization of the latter, was previously reported.[41,50] Methyl triflate (2.2 mL, 20 mmol) was added dropwise to a dark brown suspension of freshly-prepared $[Fe_2Cp_2(CO)_2(\mu\text{-}CO)(\mu\text{-}CS)]$ (17 g, *ca*. 16 mmol considering a 40 % yield from $[Fe_2Cp_2(CO)_4]$)[72,74] in anhydrous CH_2Cl_2 (80 mL) under N_2. The resulting dark brown-red mixture was stirred for 2 h at room temperature then transferred on top of an alumina column (h 8, d 6.5 cm). A dark red-brown band, containing $[Fe_2Cp_2(CO)_4]$ and other impurities, was thoroughly eluted with neat CH_2Cl_2 then a red band, containing [**1**]$^{+}$, was eluted with MeCN. Volatiles were removed under vacuum; the residue was dissolved in CH_2Cl_2 and filtered over celite. The filtrate was taken to dryness under vacuum and the residue was triturated in Et_2O (250 mL). The suspension was filtered and the resulting carmine red solid was washed with Et_2O, petroleum ether and dried under vacuum (40 °C). Yield: 5.41 g, *ca*. 63 % (*ca*. 22 % overall yield from $[Fe_2Cp_2(CO)_4]$). The title compound can be conveniently manipulated in air but it should be always stored under dry N_2 where it is stable for years. The slow, aerobic oxidation of solid [**1**]CF_3SO_3 afforded a dark red sticky solid containing a minor amount of a cationic $\{Fe^{(II)}Cp(CO)\}^{+}$ complex [IR (CH_2Cl_2): $\tilde{\upsilon}/cm^{-1}$ = 2075 cm^{-1}]. A significant decrease in yield and purity occurred when the

chromatography was performed in air and/or if using THF as eluent, due to a manifest decomposition in the column (appearance of a brown-green band containing $[Fe_2Cp_2(CO)_2(\mu\text{-}CO)(\mu\text{-}CS)]$ and $[Fe_2Cp_2(CO)_4]$). Soluble in water, MeOH, MeCN, THF, CH_2Cl_2, acetone; insoluble in Et_2O, hexane. Anal. calcd. for $C_{16}H_{13}F_3Fe_2O_6S_2$: C, 35.98; H, 2.45; S, 12.01. Found: C, 36.10; H, 2.34; S, 12.07. IR (solid state): $\tilde{\upsilon}/cm^{-1}$ = 3490w-br, 3113w, 3026w, 2936w, 2029s (CO), 1994s (CO), 1845s (μ-CO), 1605w, 1594w, 1503w, 1474w, 1430w, 1420w, 1262s (SO_3), 1253s, 1224s-sh (SO_3), 1157s (SO_3), 1142s-sh, 1117m-sh, 1070w, 1029s (μ-CS), 1016s-sh, 962m-sh, 908w, 891w, 857s, 833w-sh, 814w, 755w, 695s. IR (CH_2Cl_2): $\tilde{\upsilon}/cm^{-1}$ = 2039s (CO), 2008m-sh (CO), 1851s (μ-CO). IR (MeCN): $\tilde{\upsilon}/cm^{-1}$ = 2039s (CO), 2006m-sh (CO), 1850s (μ-CO). IR (THF): $\tilde{\upsilon}/cm^{-1}$ = 2028s (CO), 1996m-sh (CO), 1844s (μ-CO). ^{1}H NMR (acetone-d_6): δ/ppm = 5.73 (s, 5H, Cp), 5.64 (s, 5H, Cp'); 3.80 (s, 3H, SMe); no changes were observed after 14 h at room temperature. $^{13}C\{^1H\}$ NMR (acetone-d_6): δ/ppm = 408.2 (μ-CS); 252.3 (μ−CO); 207.9, 207.8 (CO); 92.9, 92.3 (Cp + Cp'); 38.0 (SMe). ^{19}F NMR (acetone-d_6): δ/ppm = − 78.8. ^{1}H NMR ($CDCl_3$): δ/ppm = 5.48, 5.41 (s+s, 10H, Cp + Cp'); 3.66 (s, 3H, SMe).

$[Fe_2Cp_2(CO)(DMAP)(\mu\text{-}CO)(\mu\text{-}CSMe)]CF_3SO_3$ ($[2]CF_3SO_3$, FETPY, Chart 3).

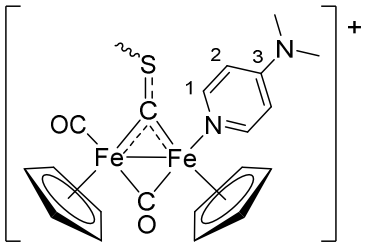

Chart 3. Structure of $[\mathbf{2}]^+$ (wavy bond refers to *E*/*Z* isomerism; numbering refers to C atoms).

Compound $[\mathbf{2}]PF_6$ was previously prepared from $[\mathbf{1}]PF_6$ by CO/4-dimethylaminopyridine (DMAP, 6 equivalents) exchange in MeCN at room temperature (6 h, 81 % yield) and characterized by IR, ^{1}H and ^{13}C NMR in acetonitrile solution.[41,48] In our hands, no reaction took place under similar conditions (1.5 eq DMAP, 24 h) and unreacted $[\mathbf{1}]CF_3SO_3$ was recovered. The CO/DMAP exchange was not particularly effective also in refluxing MeCN (*ca*. 60 % conversion after 72 h), while an extensive decomposition of the organometallic scaffold was observed in a refluxing (*ca*. 105 °C)

MeCN/toluene solution. Herein we provide a novel, effective procedure together with a complete NMR/IR characterization. A dark red solution of [**1**]CF_3SO_3 (150 mg, 0.28 mmol) and DMAP (38 mg, 0.31 mmol) in THF (5 mL) was heated at reflux under N_2. After 15 h, the resulting dark brown suspension was taken to dryness under vacuum. The crude was dissolved in few mL of CH_2Cl_2, moved on top of an alumina column (h 3, d 4.3 cm) and purified by flash chromatography (elution assisted by N_2 or air pressure – degradation products are otherwise detected in the final product). Impurities were eluted with neat THF (orange-brown band) then a brown band was eluted with MeCN/THF 1:1 *V*/*V*. Volatiles were taken to dryness under vacuum. The sticky brown residue was soaked in Et_2O/toluene 2:1 *V*/*V* (20 mL) overnight then triturated under vigorous stirring. The suspension was filtered and the resulting brown solid was washed with Et_2O/toluene 2:1 *V*/*V*, Et_2O, hexane and dried under vacuum (40 °C). Yield: 102 mg, 58 %. Soluble in MeCN, acetone, CH_2Cl_2, scarcely soluble in THF, insoluble in Et_2O, toluene, hexane. Anal. Calcd. for $C_{22}H_{23}F_3Fe_2N_2O_5S_2$: C, 42.06; H, 3.69; N, 4.46; S, 10.21. Found: C, 41.65; H, 3.60; N, 4.42; S, 10.16. IR (solid state): $\tilde{\upsilon}/cm^{-1}$ = 3103w, 2962w, 2926w, 1981s (CO), 1796s (μ-CO), 1615s, 1536s, 1445w, 1421w, 1391m, 1439w, 1258br-s (SO_3), 1233s-sh, 1222s (SO_3), 1146s (SO_3), 1064m, 1028s, 1014-1004s, 949w-sh, 844-828m-sh, 810s, 753w, 713s-sh, 700s. IR (CH_2Cl_2): $\tilde{\upsilon}/cm^{-1}$ = 2002s (CO), 1813s (μ-CO), 1627s, 1617s-sh, 1541m. IR (MeCN): $\tilde{\upsilon}/cm^{-1}$ = 1997s (CO), 1811m (μ-CO), 1627s. ^{1}H NMR (acetone-d_6): δ/ppm = 7.79 (s-br, 2H, C^{1}H); 6.39 (d, $^3J_{HH}$ = 7.4 Hz, 2H, C^{2}H); 5.35 (s, 5H, Cp); 5.08 (s, 5H, Cp'); 3.9-3.7 (br, 3H, SMe); 2.94 (s, 6H, NMe); no changes were observed after 48 h at room temperature. ^{13}C{^{1}H} NMR (acetone-d_6): δ/ppm = 266.8 (μ-CO); 210.8 (CO); 155.3 (C^3); 153.4 (br, C^1); 122.5 (d, $^1J_{CF}$ = 322 Hz, CF_3); 109.2 (C^2); 90.9 (br, Cp + Cp'); 39.0 (NMe_2); 36 (br, SMe); the μ-CS resonance was not observed even after 48 h acquisition. Numerous attempts to collect X-ray quality crystals of the title compound came unsuccessful.

[Fe_2Cp_2(CO)(κ*P*-PTA)(μ-CO)(μ-CSMe)]CF_3SO_3 ([3]CF_3SO_3, Chart 4).

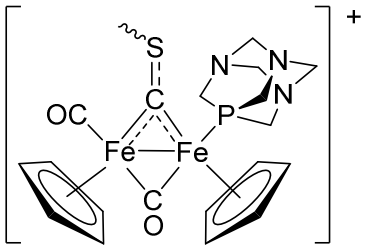

Chart 4. Structure of [**3**]$^+$ (wavy bond represents *E*/*Z* isomerism).

A dark red brown solution of [**1**]CF_3SO_3 (120 mg, 0.22 mmol) and 1,3,5-triaza-7-phosphaadamantane (PTA, 36 mg, 0.22 mmol) in deaerated THF (10 mL; 12 mg [**1**]CF_3SO_3/mL) was heated at reflux under N_2 for 1 h. The resulting mixture (dark green solution + solid) was cooled to – 20 °C. The cold suspension was filtered; the resulting dark green solid was washed with cold THF (5 mL), Et_2O, petroleum ether and dried under vacuum. Yield = 118 mg, 70 %. By-products were observed in the isolated solid when the reaction was carried out in a more concentrated solution (> 60 mg [**1**]CF_3SO_3/mL). Soluble in DMSO, less soluble H_2O, MeOH, MeCN, acetone; poorly soluble in ^{i}PrOH, CH_2Cl_2, THF, insoluble in Et_2O. Crystals of [**3**]$CF_3SO_3 \cdot (H_2O)_{2.33}$ suitable for X-ray analysis were obtained from an acetone solution layered with Et_2O and settled aside at – 20 °C. Anal. calcd. for $C_{21}H_{25}F_3Fe_2N_3O_5PS_2$: C, 38.03; H, 3.80; N, 6.34; S, 9.67. Found: C, 37.90; H, 3.74; N, 6.12; S, 9.80. IR (solid state): $\tilde{\upsilon}$/cm^{-1} = 3519w, 3360w-br, 3109w, 2981-2886w, 1969s (CO), 1798s (μ-CO), 1450w, 1422w, 1411w, 1275s-sh, 1257s (SO_3), 1244s-sh, 1225m-sh (SO_3), 1158s (SO_3), 1144s, 1103m, 1030s, 1016s, 980m, 970m, 950s, 895w, 852m, 866m-sh, 804w, 747w, 692s. IR (CH_2Cl_2): $\tilde{\upsilon}$/cm^{-1} = 1984s (CO), 1816s (μ-CO). IR (MeCN): $\tilde{\upsilon}$/cm^{-1} = 1984s (CO), 1816s (μ-CO). ^{1}H NMR (CD_3OD): δ/ppm = 5.35, *5.28* (s-br, 5H, Cp); *5.22*, 5.17 (s-br, 5H, Cp^P); 4.44–4.32 (m-br, 6H, NCH_2); 3.90–3.75 (m-br, 6H, PCH_2); *3.60*, 3.53 (s, 3H, SMe); isomer (*cis*-*E*/*cis*-*Z*) ratio = 2. ^{13}C{^{1}H} NMR (CD_3OD): δ/ppm = 409.8 (d, $^2J_{CP}$ = 13 Hz, μ-CS); 256 (d, $^2J_{CP}$ ≈ 10 Hz, μ-CO); 215.6 (CO); 121.8 (d, $^1J_{CF}$ = 319 Hz, CF_3); *91.8*, 90.8, 90.7, *89.8* (Cp + Cp^P); 72.8 (d, $^3J_{CP}$ = 6 Hz, NCH_2); *54.3* (d, $^1J_{CP}$ = 12 Hz), 53.3 (d, $^1J_{CP}$ = 14 Hz) (PCH_2); *37.1*, 36.7 (SMe). ^{19}F NMR (CD_3OD): δ/ppm = − 80.1. ^{31}P{^{1}H} NMR (CD_3OD): δ/ppm = − 17.5, − *26.6*. ^{1}H NMR (acetone-d_6): δ/ppm = 5.48, *5.39* (s-br, 5H, Cp); *5.36*, 5.30 (s-br, 5H, Cp^P); 4.37 (s, 6H, NCH_2); *3.98*, 3.91 (s, 6H, PCH_2); *3.72*, 3.61 (s, 3H, SMe); isomer (*cis*-*E*/*cis*-*Z*) ratio ≈ 2. ^{31}P{^{1}H} NMR (acetone-d_6): δ/ppm = − 18.5, − *27.7*. ^{1}H NMR

(DMSO-d_6): δ/ppm = 5.39, *5.33* (s-br, 5H, Cp); *5.26*, 5.23 (s-br, 5H, Cp'); 4.32–4.21 (m-br, 6H, NCH_2), 3.81–3.64 (m-br, 6H, PCH_2); *3.57*, 3.47 (s-br, 3H, SMe); isomer (cis-*E*/cis-*Z*) ratio = 1.7. $^{13}C\{^1H\}$ NMR (DMSO-d_6): δ/ppm = 406.7 (m), *400.4* (d, $^2J_{CP}$ = 15 Hz) (μ-CS); 260.8 (m), 257.6 (d, $^2J_{CP}$ = 14 Hz) (μ-CO); 214.8, *214.7* (CO); 120.7 (q, $^1J_{CF}$ = 322 Hz, CF_3); *90.6*, 89.7, 89.6, *88.9* (Cp + Cp^P); 71.3 (d, $^3J_{CP}$ = 7 Hz, NCH_2); *52.7* (m), 51.8 (d, $^1J_{CP}$ = 12 Hz) (PCH_2); *36.4*, 36.2 (SMe). $^{31}P\{^1H\}$ NMR (DMSO-d_6): δ/ppm = − 15.2, − *25.0*.

4.3. X-Ray Crystallography

Crystal data and collection details for [**3**]$CF_3SO_3 \cdot (H_2O)_{2.33}$ are reported in Table S2. Data were recorded on a Bruker APEX II diffractometer equipped with a PHOTON2 detector using Mo–Kα radiation. Data were corrected for Lorentz polarization and absorption effects (empirical absorption correction SADABS).[82] The structure was solved by direct methods and refined by full-matrix least-squares based on all data using F^2.[83] Hydrogen atoms were fixed at calculated positions and refined by a riding model, except those of H_2O molecules that have been located in the Fourier difference map and refined isotropically with restrained O-H distances. All non-hydrogen atoms were refined with anisotropic displacement parameters. The asymmetric unit of the unit cell contains two independent molecules, both showing disorder of the μ-CO and μ-CSMe ligands. Despite the disorder, the Me group bonded to S lies always in the same side of the PTA ligand (cis-Z isomer).

4.4. Biological Studies

Reagents

Reagents have been purchased from following manufacturers: Capricorn Scientific GmbH (Hessen, Germany) – Fetal bovine serum (FBS) and culture mediums RPMI 1640, with L-Glutamine, with 25 mM HEPES and Dulbecco's Modified Eagle Medium (DMEM); Sigma Aldrich (St. Louis, MO, USA) – Ethylenediaminetetraacetic acid (EDTA), trypsin, phosphate-buffered saline (PBS), dimethyl sulfoxide (DMSO), ribonuclease (RNase) A, carboxyfluoresceindiacetate succinimidyl ester (CFSE), dihydroethidium (DHE), propidium iodide (PI), ExtrAvidin Peroxidase Staining Kit for rabbit

antibodies (EXTRA 3), 3,4-Dihydroxy-L-phenylalanine (L-DOPA), Anti-Mouse IgG – Biotin antibody produced in goat, chloroquine, apocynin and acridine orange (AO), Crystal violet (CV); Biological Industries (Cromwell, CT, USA) – The Penicillin Streptomycin solution; Serva (Heidelberg, Germany) – Paraformaldehyde (PFA); AppliChem (MO, USA) – 3 (4,5 dimethythiazol-2-yl)-2,5-diphenyltetrazolium bromide (MTT); BD (Pharmingen, San Diego, SAD) – Annexin V-FITC (AnnV); R&D Systems (Minneapolis, MN, USA) – ApoStat; Thermo Fisher Scientific (Waltham, MA, USA) – Dihydrorhodamine 123 (DHR); Lach-Ner (Neratovice, Czechia) – Sodium hydroxide (NaOH); Dako (Glostrup, Denmark) – Liquid DAB substrate chromogen system, Glycergel mounting medium; BioOptica (Milan, Italy) – Mayer's hematoxylin, Oil red O solution; Zorka (Šabac, Serbia) – Methanol, ethanol, acetic acid, hydrogen peroxyde (H_2O_2); Fluka (Buchs, Switzerland) – Triton X-100, trypan blue; BioLegend (San Diego, CA, USA) – Purified anti-myelin basic protein antibody; Cayman Chemical (Ann Arbor, MI, USA) – C11 BODIPY 581/591, ferrostatin-1; Fisher Scientific (Hampton, NH, USA) – Bovine serum albumin (BSA); Enzo Life Sciences (Farmingdale, NY, USA) – Diaminofluorescein (DAF) FM diacetate.

Cells

Human cell lines (A2780, MCF7, HCT 116, MRC5) and mouse cell lines (B16-F1, B16-F10, 4T1, CT26, NIH 3T3) were obtained from the American Type Culture Collection (Rockville, MD, USA). All cell lines, except NIH 3T3, were cultivated in HEPES-buffered RPMI-1640 medium, while NIH 3T3 cells were cultivated in DMEM. Both mediums were supplemented with 10% heat-inactivated FCS, penicillin (100 units/mL), and streptomycin (100 μg/mL). Cells were cultivated in a humidified atmosphere with 5% CO_2, at 37 °C.

Viability assays (MTT and CV)

Cells were seeded overnight in 96-well plates using following densities: A2780 and MRC5 $8 \cdot 10^3$ cells/well, MCF7 $10 \cdot 10^3$ cells/well, HCT 116 and NIH 3T3 $6 \cdot 10^3$ cells/well, B16-F1 $4 \cdot 10^3$ cells/well, 4T1 $3 \cdot 10^3$ cells/well and B16-F10 $2 \cdot 10^3$ cells/well. The next day, cells were treated with different concentrations of diiron complexes. Viability assays were conducted after 72 hours of treatment.

For the MTT assay, cells were washed with PBS and cultivated in the presence of MTT solution (0.5 mg/mL) for 45 min – 1 hour at 37 °C, until purple formazan crystals were formed. MTT solution was then discarded and DMSO was added to dissolve formazan crystals. The absorbance of the solution was measured at 540 nm. For CV assay, cells were washed with PBS and fixed with 4% PFA at RT for 10 minutes. After that, cells were stained with 1% CV solution for 15 minutes at RT, then washed in tap water and dried. Before absorbance measuring, the dried dye was dissolved in 33% acetic acid. The absorbance of the solution was measured at 540 nm. Cell viability was calculated as a percentage of control set to 100%. To determine the outcome of induced autophagy, B16-F1 cells were treated with IC_{50} of [**2**]CF_3SO_3, with or without autophagy inhibitor chloroquine (20 μM). The viability of B16-F1 cells was assessed by CV assay. In order to determine whether NADPH oxidase 2 (NOX2) enzyme is a potential target of [**2**]CF_3SO_3, B16-F10 cells were treated with IC_{50} of this complex, with or without NOX2 inhibitor apocynin (25 μM). Cell viability was assessed by CV assay.

Cellular iron content

Microwave digestion. The digestion of the samples was performed on Advanced Microwave Digestion System (Ethos 1, Milestone, Italy) using HPR-1000/10S high-pressure segmented rotor. The pressure-resistant PTFE vessels (volume 100 ml) which were equipped with QS-50 Quartz inserts, were used. The sample was precisely placed in the quartz insert and mixed with of 4 ml HNO_3 (65 wt%, Suprapur®) and 0.5 ml H_2O_2 (30 wt.%, Suprapur®) (both of Merck KGaA, Darmstadt, Germany). The temperature was gradually raised with microwave power (0-1000 W): linearity from 25 to 180 ºC in the first 15 min, remained at 180 ºC in the next 20 min, and then decreased rapidly to room temperature. After cooling and without filtration, the solution was diluted to a fixed volume (5 ml) in the volumetric flask with ultrapure water. Ultrapure water with a conductivity of 0.05 μS/cm was prepared using a Barnstead™ GenPure™ Pro (Thermo Scientific, Germany).

ICP-OES measurement. The contents of the iron total in solution samples was determined by inductively coupled plasma optical emission spectrometry, ICP-OES (iCAP 6500 Duo ICP, Thermo Fisher Scientific, Cambridge, United Kingdom). The external calibration solutions were made from

the certified plasma standard solution: Multi-Element Plasma Standard Solution 4, Specpure®, 1000 µg/ml (Alfa Aesar GmbH & Co KG, Germany. Quality control was carried out using blank samples, matrix-matched calibration solutions and duplicate analyses of each sample. The analytical process quality control, performed by the use of certified reference material (CRM) of fish protein for trace metals DORM 4 (NRCC, National Research Council Canada, Ottawa, Ontario Canada). Recovery of measured concentration of the iron with certified value was 99.6%. Concentration of iron of the sample was expressed as ng(Fe)/$1 \cdot 10^6$ cells.

Flow cytometry

To perform flow cytometry analysis, cells were seeded overnight in 6-well plates using following densities: A2780 $3 \cdot 10^5$ cells/well, B16-F1 $1 \cdot 10^5$ cells/well and B16-F10 $0.5 \cdot 10^5$ cells/well (except for detection of ferroptosis). The next day, cells were treated with IC_{50} of [**2**]CF_3SO_3 for 48 hours (A2780, except for CFSE staining 72h) or 72 hours (B16-F1 and B16-F10). For apoptosis detection, cells were stained with 1.35 µg/mL AnnV and 15 µg/mL PI for 15 minutes at RT, protected from the light. Cells were then resuspended in AnnV-binding buffer and analyzed. In order to detect potential caspase activation, cells were incubated with 0.5 µg/mL pan-caspase inhibitor Apostat for 30 minutes at 37 °C. After that, cells were washed with PBS and analyzed. For detection of autophagy, cells were stained with 10 µM acridine orange for 15 minutes at 37 °C, then washed with PBS and analyzed. To investigate the potential effect of [**2**]CF_3SO_3 on cell proliferation, cells were stained with 1 µM CFSE for 10 minutes at 37 °C and washed with PBS, just before seeding. The day after, cells were treated with IC_{50} of [**2**]CF_3SO_3 for 72 hours. Finally, cells were washed with PBS, trypsinized, resuspended in PBS, and analyzed. For detection of intracellular hydrogen peroxide and peroxynitrite production, cells were stained with 1 µM DHR 123 for 20 minutes at 37 °C, then seeded and treated the next day with IC_{50} of [**2**]CF_3SO_3. After that, cells were washed with PBS, trypsinized, resuspended in PBS, and analyzed. For detection of intracellular superoxide anion production, cells were seeded, treated with [**2**]CF_3SO_3, as described previously, and then stained with 20 µM DHE for 45 minutes at RT

before analysis. In order to detect intracellular NO production, cells were seeded, treated with [**2**]CF_3SO_3 the next day, and after the incubation period stained with 1 μM DAF-FM for 1 hour in medium without phenolphthalein at 37 °C. Cells were then washed with PBS, incubated with medium without FBS and phenolphthalein for 15 minutes at 37 °C, trypsinized, resuspended in PBS, and analyzed. For ferroptosis detection, cells were seeded in 24-well plates, using following densities: A2780 $30 \cdot 10^3$ cells/well, B16-F1 $50 \cdot 10^3$ cells/well, and B16-F10 $20 \cdot 10^3$ cells/well. The next day, cells were treated with IC_{50} of [**2**]CF_3SO_3 with or without 2 μM ferrostatin-1. After 48 hours (A2780) and 72 hours (B16-F1 and B16-F10) of treatment, cells were stained with 2 μM BODIPY 581/591 for 30 minutes, washed, resuspended in PBS and analyzed.

Microscopy

For microscopic analysis, cells were seeded in 8-well chambers, using following densities: A2780 $20 \cdot 10^3$ cells/well, B16-F1 $15 \cdot 10^3$ cells/well and B16-F10 at $8 \cdot 10^3$ cells/well. Microscope slides were analysed using Zeiss AxioObserver Z1 microscope (Carl Zeiss AG, Oberkochen, Germany) at 40 × magnification.

PI staining

After 48 h (A2780) or 72 h (B16-F1 and B16-F10) of treatment with IC_{50} of [**2**]CF_3SO_3, cells were washed with PBS and then fixed with 4% PFA for 15 min at room temperature. After fixation, cells were washed in distilled water and stained with PI solution for 2 minutes. The PI solution contains 50 μg/mL of PI, Triton X-100 (0.1%), EDTA pH 8.0 (0.1 mM), and 50 μg/mL of RNase in PBS. After staining, fluorescent mounting medium was used to cover the cells. Finally, coverslips are placed over the mounting medium.

Oil red staining

After 72 hours of treatment with IC_{50} of [**2**]CF_3SO_3, B16-F1 and B16-F10 cells were washed with PBS and then fixed with 4% PFA for 15 min at room temperature. After fixation, cells were washed with PBS one more time and stained with Oil red O solution for 20 minutes at room temperature.

Cells were then washed with tap water, dried and stained with hematoxylin for 30 seconds. Once again, cells were washed in tap water, dried and covered with an aqueous mounting medium. Finally, coverslips are placed over the mounting medium.

Myelin basic protein (MBP) antibody staining

After 72 hours of treatment with IC_{50} of [**2**]CF_3SO_3, B16-F1 and B16-F10 cells were washed with PBS and then fixed with 4% PFA for 15 min at room temperature. Cells were incubated with 0.5% Triton X-100 in PBS (PBST) for 30 minutes, washed with PBS, and then incubated with 3% H_2O_2 in 10% methanol in 0.5% PBST for 10 minutes in a moist chamber. After washing with PBS, cell non-specific binding sites were blocked by incubation with 5% FBS in 0.1% PBST for 1 hour in a moist chamber at room temperature. Once again, cells were washed with PBS and incubated with 1° antibody diluted in 1% BSA in PBS (for negative control 1% BSA in PBS without antibody) at 4 °C in a moist chamber, overnight. The next day, cells were washed with PBS and incubated with bionylated 2° antibody diluted in 1% BSA in PBS for 30 minutes in a moist chamber, at room temperature. After washing with PBS, cells were incubated with extravidin peroxidase – HRP diluted in 1% BSA in PBS for 30 minutes in a moist chamber, at room temperature. Cells were washed with PBS, incubated with DAB substrate, and watched under the microscope until color was developed. After color is developed, the reaction is stopped by washing with PBS. Cells were incubated with Mayers' hematoxylin for 30 seconds for contrast staining, washed in tap water until color is developed, and then washed in distilled water. After drying, cells were covered with a mounting medium. Finally, coverslips are placed over the mounting medium.

Melanin content and tyrosinase activity assays

Cells were seeded in 6-well plate, using following densities: B16-F1 $1 \cdot 10^5$ cells/well and B16-F10 $0.5 \cdot 10^5$ cells/well. The next day, cells were exposed to the IC_{50} of [**2**]CF_3SO_3 for 72 h. Live cells were collected, counted and then the same number of untreated and treated cells was used for both assays. Cells were centrifuged at 2000 rpm for 5 minutes. To determine melanin content, cells were lysed in

1 M NaOH, mixed with distilled water, and incubated for 1 hour at 60 °C. After the incubation, absorbance was measured at 492 nm. To determine tyrosinase activity, cells were lysed in PBS pH 6.8 – 1% Triton X-100. After the centrifuge at 10 000 rpm for 5 minutes, supernatant was mixed with L-DOPA substrate solution (2 mg/mL) and incubated for 30 minutes at 37 °C. The absorbance was measured at 540 nm.

In vivo experiments

Eight to twelve weeks old C57BL/6 male or female mice were obtained from the facility of the Institute for Biological Research "Siniša Stanković" (IBISS), University of Belgrade, Serbia and used for the *in vivo* experiments. Animals were kept in the standard (non-specific pathogen-free) breeding conditions. They had free access to food and water. The study protocols and handling of animals were in agreement with the rules of the EU guidelines. Experiments were approved by the Veterinary Directorate, the entity of the Ministry of Agriculture, Forestry and Water Management in Belgrade, Serbia (323-07-03379/2023-05, 323-07-08047/2023-05). For the therapeutic *in vivo* model of mouse melanoma, 1.8×10^5 of B16-F1 or B16-F10 cells/100 µL PBS were inoculated subcutaneously into dorsal right flank of each animal, respectively. During the inoculation, animals were anesthetized with isoflurane (3%) via inhalation. Treatment started after 7-10 days, when tumors became palpable. One group was treated with 4 mg/kg of [**2**]CF_3SO_3 in 400 µL of 2% DMSO/PBS per animal, every day, via intraperitoneal (i.p.) injection. The other group received only solvent, every day, via i.p. injection. The number of animals per group was 10. When tumor volume reached approximately 10% of animal's body weight, mice were euthanized and tumor, liver and kidney tissues were collected for histopathological analysis. During the experiment, tumor size was measured twice a week and the volume was calculated by the formula: length × width^2 × 0.52 (mm^3). Animal welfare was closely monitored for signs of toxicity every day. Additionally, animals' weight and urine samples were measured and collected once a week. To investigate the tumorigenic potential of *in vitro* treated B16-F1 or B16-F10 *in vivo*, $1 \cdot 10^5$ of B16-F1 or B16-F10 cells/100 µL PBS were inoculated

subcutaneously into the dorsal right flank of each animal, respectively. One group received collected live B16-F1 or B16-F10 cells previously treated *in vitro* with IC_{50} of [**2**]CF_3SO_3 for 72 h, while the other group received untreated B16-F1 or B16-F10 cells, respectively. During the inoculation, animals were anesthetized with isoflurane (3%) via inhalation. The number of animals per group was 10. Tumor growth was monitored and measured twice a week. Tumor volume was calculated by the formula: length × width^2 × 0.52 (mm^3). Animal welfare was closely monitored every day. When tumor volume reached approximately 10% of the animal's body weight, mice were euthanized.

Histopathological Analysis

Sacrificed animal tissues (tumor, liver, and kidney) were examined, measured, and cut into 3 mm thick slices. Tissues were processed using automated equipment (Milestone SRL LOGOS ONE, Sorisole, BG–Italy). Paraffin embedding was performed on an embedding console (SAKURA TissueTek TEC 5, Sakura Finetek, CA, USA). Thin 4 μm sections were cut using a microtome ((LEICA RM 2245, Leica Biosystems, Nussloch, Germany) and mounted on glass slides. These slides were stained with hematoxylin and eosin. Microscopic analysis was carried out using an Olympus BX43 microscope, and all slides were digitally scanned using a Leica Aperio AT2 slide scanner for documentation. Morphometric analysis was conducted using Leica Aperio ImageScope software.

Statistical Analysis

The presented data represent the means ± standard deviation (SD) of at least three independent experiments. Student *t*-test, one-way ANOVA and non-parametric Mann–Whitney test were used to evaluate the significance between tested groups. Statistical significance was indicated if two-sided *p*-values were less than 0.05.

Conflicts of interest. The authors declare no competing financial interest.

Acknowledgements. We thank the Ministry of Science, Technological Development and Innovation of the Republic of Serbia (No. 451-03-47/2023-01/200007) and the University of Pisa (Fondi di Ateneo 2020) for funding. We are grateful to Prof. Valerio Zanotti (University of Bologna) for providing valuable suggestions related to the synthetic work.

Alphabetical list of abbreviations and acronyms.

B16-F1, low-invasive mouse melanoma cells; B16-F10, high-invasive mouse melanoma cells; C57BL/6, C57 black 6, common inbred strain of laboratory mouse; IRP1, iron regulatory protein 1; IRP2, iron regulatory protein 2; TfR1, transferrin receptor 1; ROS, reactive oxygen species; HCT 116, human colorectal carcinoma cells; MCF7, human breast cancer cells; A2780, human ovarian cancer cells; MRC5, human fetal lung fibroblasts; CV, crystal violet; BODIPY, 4,4-difluoro-4-bora-3a,4a-diaza-s-indacene; DHR123, dihydrorhodamine 123, methyl 2-(3,6-diamino-9H-xanthen-9-yl)benzoate; Benzoic acid, 2-(3,6-diamino-9H-xanthen-9-yl)-, methyl ester; DHE, dihydroethidium, 2,7-Diamino-10-ethyl-9-phenyl-9,10-dihydrophenanthridine, 3,8-Diamino-5,6-dihydro-5-ethyl-6-phenylphenanthridine; DAF-FM, DAF-FM diacetate (4-amino-5-methylamino-2',7'-difluorofluorescein diacetate); RNS, reactive nitrogen species; NADPH, nicotinamide-adenine dinucleotide phosphate; NOX2, NADPH oxidase 2 (nicotinamide adenine dinucleotide phosphate oxidase 2); δ, chemical shift in parts per million downfield from tetramethylsilane; μ, micro; Å, angstrom(s); °C, degrees Celsius; 3D, three-dimensional; aq, aqueous; BODIPY, ; BSA, bovine serum albumin; COSY, COrrelated SpectroscopY; Cp, cyclopentadienyl; Cy, Cyclohexyl; DMAP, 4-dimethylaminopyridine; DMSO, Dimethyl sulfoxide; DMEM, Dulbecco's Modified Eagle's Medium; FT-IR, Fourier Transformed Infrared Spectroscopy; gs-HSQC, Gradient Selective Heteronuclear Single Quantum Coherence Spectroscopy; HR-ESI-MS, High Resolution Electron Spray Ionization Mass Spectroscopy; IC_{50}, concentration that causes 50% inhibition of cell proliferation; ICP-OES, Inductively Coupled Plasma – Optical Emission Spectroscopy; Log P_{ow}, octanol-water partition coefficient; Me, Methyl; MTT, (3-(4,5 dimethylthiazol-2-yl)2,5-diphenyl-

tetrazolium bromide); NER, nucleotide excision repair; NOESY, Nuclear Overhauser Effect Spectroscopy; NMR, Nuclear Magnetic Resonance; ORTEP, Oak Ridge Thermal Ellipsoid Plot; PBS, phosphate-buffered saline; PI, Propidium Iodide; ppm, part(s) per million; PMMA, polymethyl methacrylate; PTA, 1,3,5-triaza-7-phosphaadamantane; RAPTA, Ruthenium Arene 1,3,5-triaza-7-phosphaadamantane complexes; RT, Room Temperature; SD, standard deviation; SI, selectivity index; UATR, Universal Attenuated Total Reflectance Accessory.

Conflicts of interest. The authors declare no competing financial interest.

Supplementary Materials. IR, NMR and MS spectra; X-ray crystallography; experiments in aqueous media; biological studies. Molecular Formula Strings. CCDC reference number 2323915 ([**3**]CF_3SO_3) contains the supplementary crystallographic data for the X-ray study reported in this paper. These data can be obtained free of charge at https://www.ccdc.cam.ac.uk/structures/ (or from the Cambridge Crystallographic Data Centre, 12, Union Road, Cambridge CB2 1EZ, UK; fax: (internat.) +44-1223/336-033; e-mail: deposit@ccdc.cam.ac.uk). Authors will release the atomic coordinates upon article publication.

References

1 B. A. Chabner, T. G. Roberts Jr, Chemotherapy and the war on cancer, Nat. Rev. Cancer 2005, 5, 65–72.

2 S. Dilruba, G. V. Kalayda, Platinum-based drugs: past, present and future, Cancer Chemother. Pharmacol. 2016, 77, 1103–1124.

3 R. Oun, Y. E. Moussa, N. J. Wheate, The side effects of platinum-based chemotherapy drugs: a review for chemists, Dalton Trans. 2018, 47, 6645–6653.

4 K. Peng, B.-B. Liang, W. Liu, Z.-W. Mao, What blocks more anticancer platinum complexes from experiment to clinic: Major problems and potential strategies from drug design perspectives, Coord. Chem. Rev. 2021, 449, 214210.

5 E. J. Anthony, E. M. Bolitho, H. E. Bridgewater, O. W. L. Carter, J. M. Donnelly, C. Imberti, E. C. Lant, F. Lermyte, R. J. Needham, M. Palau, P. J. Sadler, H. Shi, F.-X. Wang, W.-Y. Zhang, Z. Zhang, Metallodrugs are unique: opportunities and challenges of discovery and development, Chem. Sci., 2020, 11, 12888–12917.

6 B. S. Murray, P. J. Dyson, Recent progress in the development of organometallics for the treatment of cancer, Curr. Opinion Chem. Biol. 2020, 56, 28-34.

7 Y. Ching Ong, G. Gasser, Organometallic compounds in drug discovery: Past, present and future, Drug Discov. Today 2020, 37, 117-124.

8 R. Crichton, The essential role of iron in biology, in Iron Metabolism: From Molecular Mechanisms to Clinical Consequences, (Eds: R. Crichton), Chichester, UK: Wiley, 2016, pp. 22–70.

9 L. C. Kühn, Iron regulatory proteins and their role in controlling iron metabolism, Metallomics 2015, 7, 232-243.

10 S. V. Torti, D. H. Manz, B. T. Paul, N. Blanchette-Farra, F. M. Torti, Iron and Cancer, Annu Rev Nutr. 2018, 38, 97-125.

11 R. E. Weinstein, B. H. Bond, B. K. Silberberg, C. B. Vaughn, P. Subbaiah, D. R. Pieper, Tissue ferritin concentration and prognosis in carcinoma of the breast, Breast Cancer Res Treat. 1989, 14, 349-353.

12 M. C. Kew, J. D. Torrance, D. Derman, M. Simon, G. M. Macnab, R. W. Charlton, T. H. Bothwell, Serum and tumour ferritins in primary liver cancer, Gut. 1978, 19, 294-299.

13 Z. Chen, W. Wang, S. R. Abdul Razak, T. Han, N. H. Ahmad, X. Li, Ferroptosis as a potential target for cancer therapy, Cell Death Dis. 2023, 14, 460.

14 D. Basuli, L. Tesfay, Z. Deng, B. Paul, Y. Yamamoto, G. Ning, W. Xian, F. McKeon, M. Lynch, C. P. Crum, P. Hegde, M. Brewer, X. Wang, L. D. Miller, N. Dyment, P. M. Torti, S. V. Torti, Iron addiction: a novel therapeutic target in ovarian cancer, Oncogene 2017, 36, 4089-4099.

15 Z. K. Pinnix, L. D. Miller, W. Wang, R. D'Agostino Jr,, T. Kute, M. C. Willingham, H. Hatcher, L. Tesfay, G. Sui, X. Di, S. V. Torti, F. M. Torti, Ferroportin and iron regulation in breast cancer progression and prognosis, Sci Transl Med. 2010, 2, 43-56.

16 G. Lei, L. Zhuang, B. Gan, Targeting ferroptosis as a vulnerability in cancer, Nat. Rev. Cancer 2022, 22, 381–396.

17 B. R: Stockwell, Ferroptosis turns 10: Emerging mechanisms, physiological functions, and therapeutic applications, Cell 2022, 185, 2401-2421.

18 J. Li, F. Cao, H.-L. Yin, Z.-J. Huang, Z.-T. Lin, N. Mao, B. Sun, G. Wang, Ferroptosis: past, present and future, Cell Death Dis. 2020, 11, 88.

19 M. Conrad, D. A. Pratt, The chemical basis of ferroptosis, Nat. Chem. Biol. 2019, 15, 1137–1147.

20 M. Morales, X. Xue, Targeting iron metabolism in cancer therapy, Theranostics 2021, 11, 8412–8429.

21 M. Patra, G. Gasser, The medicinal chemistry of ferrocene and its derivatives, Nat. Chem. Rev. 2017, 1, 0066.

22 R. Wang, H. Chen, W. Yan, M. Zheng, T. Zhang, Y. Zhang, Ferrocene-containing hybrids as potential anticancer agents: Current developments, mechanisms of action and structure-activity relationships, Eur. J. Med. Chem. 2020, 190, 112109.

23 A. Vessières, Y. Wang, M. J. McGlinchey, G. Jaouen, Multifaceted chemical behaviour of metallocene (M = Fe, Os) quinone methides. Their contribution to biology, Coord. Chem. Rev. 2021, 430, 213658.

24 T. W. Johnson, R. A. Gallego, M. P. Edwards, Lipophilic Efficiency as an Important Metric in Drug Design, J. Med. Chem. 2018, 61, 6401 – 6420.

25 X. Liu, B. Testa, A. Fahr, Lipophilicity and Its Relationship with Passive Drug Permeation, Pharm Res 2011, 28, 962-977.

26 M. Chen, J. Borlak, W. Tong, high lipophilicity and high daily dose of oral medications are associated with significant risk for drug-induced liver injury, Hepatology 2013, 58, 388-396.

27 C. B. van Beek, N. P. van Leest, M. Lutz, S. D. de Vos, R. J. M. Klein Gebbink, B. de Bruin, D. L. J. Broere, Combining metal–metal cooperativity, metal–ligand cooperativity and chemical non-innocence in diiron carbonyl complexes, Chem. Sci. 2022, 13, 2094-2104.

28 J. Campos, Bimetallic cooperation across the periodic table, Nat. Rev. Chem. 2020, 4, 696–702.

29 V. Ritleng, M. J. Chetcuti, Hydrocarbyl Ligand Transformations on Heterobimetallic Complexes. Chem. Rev. 2007, 107, 797−858.

30 W. Lubitz, H. Ogata, O. Rüdiger, E. Reijerse, Chem. Rev. 2014, 114, 4081−4148. b) J. T. Kleinhaus, F. Wittkamp, S. Yadav, D. Siegmund, U.-P. Apfel, [FeFe]-Hydrogenases: maturation and reactivity of enzymatic systems and overview of biomimetic models, Chem. Soc. Rev. 2021, 50, 1668-1784.

31 Y. Li, T. B. Rauchfuss, Synthesis of Diiron(I) Dithiolato Carbonyl Complexes, Chem. Rev. 2016, 116, 7043-7077.

32 S. Gao, Y. Liu, Y. Shao, D. Jiang, Q. Duan, Iron carbonyl compounds with aromatic dithiolate bridges as organometallic mimics of [FeFe] hydrogenases, Coord. Chem. Rev. 2020, 402, 213081.

33 L. Biancalana, F. Marchetti, Aminocarbyne ligands in organometallic chemistry, Coord. Chem. Rev. 2021, 449, 214203.

34 F. Marchetti, Constructing Organometallic Architectures from Aminoalkylidyne Diiron Complexes, Eur. J. Inorg. Chem. 2018, 3987–4003.

35 F. Arrigoni, L. Bertini, L. De Gioia, A. Cingolani, R. Mazzoni, V. Zanotti, G. Zampella, Mechanistic Insight into Electrocatalytic H_2 Production by $[Fe_2(CN)\{\mu\text{-}CN(Me)_2\}(\mu\text{-}CO)(CO)(Cp)_2]$: Effects of Dithiolate Replacement in [FeFe] Hydrogenase Models, Inorg. Chem. 2017, 56, 13852-13864.

36 C. Saviozzi, S. Stocchetti, G. Bresciani, L. Biancalana, G. Pampaloni, F. Marchetti, Adding Diversity to Diiron Aminocarbyne Complexes with Amine Ligands, Inorganics 2023, 11, 91.

37 R. Mazzoni, A. Gabiccini, C. Cesari, V. Zanotti, I. Gualandi, D. Tonelli, Diiron Complexes Bearing Bridging Hydrocarbyl Ligands as Electrocatalysts for Proton Reduction, Organometallics 2015, 34, 3228−3235.

38 C. Saviozzi, L. Biancalana, T. Funaioli, M. Bortoluzzi, M. De Franco, M. Guelfi, V. Gandin, F. Marchetti, Inorg. Chem. 2024, 63, 2, 1054–1067, Triiron Complex with N-Ferrocenyl Aminocarbyne Ligand Bridging a Diiron Core: DFT, Electrochemical, and Biological Insights, Inorg. Chem. 2024, 63, 1054–1067

39 B. Campanella, S. Braccini, G. Bresciani, M. De Franco, V. Gandin, F. Chiellini, A. Pratesi, G. Pampaloni, L. Biancalana, F. Marchetti, The choice of μ-vinyliminium ligand substituents is key to optimize the antiproliferative activity of related diiron complexes, Metallomics 2023, 15, mfac096.

40 L. Biancalana, M. De Franco, G. Ciancaleoni, S. Zacchini, G. Pampaloni, V. Gandin, F. Marchetti, Easily Available, Amphiphilic Diiron Cyclopentadienyl Complexes Exhibit in Vitro Anticancer Activity in 2D and 3D Human Cancer Cells through Redox Modulation Triggered by CO Release, Chem. Eur. J. 2021, 27, 10169-10185.

41 M. H. Quick, R. J. Angelici, Substitution and S-alkylation reactions of thiocarbonyl-bridged $Cp_2Fe_2(CO)_3CS$, Inorg. Chem. 1981, 20, 1123-1130.

42 L. Busetto, V. Zanotti, Thiocarbonyl, thiocarbyne and thiocarbene ligands in di-and polynuclear complexes, Inorg. Chim. Acta 2008, 361, 3004–3011, and references therein.

43 G. Agonigi, L. Biancalana, M. G, Lupo, M. Montopoli, N. Ferri, S. Zacchini, F. Binacchi, T. Biver, B. Campanella, G. Pampaloni, V. Zanotti, F. Marchetti, Exploring the Anticancer Potential of Diiron Bis-cyclopentadienyl Complexes with Bridging Hydrocarbyl Ligands: Behavior in Aqueous Media and In Vitro Cytotoxicity, Organometallics 2020, 39, 645-657.

44 L. Biancalana, M. Kubeil, S. Schoch, S. Zacchini, F. Marchetti, Switching on Cytotoxicity of Water-Soluble Diiron Organometallics by UV Irradiation, Inorg. Chem. 2022, 61, 7897-7909.

45 R. Mejia-Rodriguez, D. Chong, J. H. Reibenspies, M. P. Soriaga, M. Y. Darensbourg, The Hydrophilic Phosphatriazaadamantane Ligand in the Development of H_2 Production Electrocatalysts: Iron Hydrogenase Model Complexes, J. Am. Chem. Soc. 2004, 126, 12004-12014.

46 J. Bravo, S. Bolaño, L. Gonsalvi, M. Peruzzini, Coordination chemistry of 1,3,5-triaza-7-phosphaadamantane (PTA) and derivatives. Part II. The quest for tailored ligands, complexes and related applications, Coord. Chem. Rev. 2010, 254, 555-607.

47 M. Rausch, P. J. Dyson, P. Nowak-Sliwinska, Recent Considerations in the Application of RAPTA-C for Cancer Treatment and Perspectives for Its Combination with Immunotherapies, Adv. Therap. 2019, 2, 1900042.

48 N. C. Schroeder, R. Funchess, R. A. Jacobson, R. J. Angelici, Reactions of $Cp_2Fe_2(CO)_2(\mu\text{-}CO)(\mu\text{-}CSR)^+$ bridging-carbyne complexes with nucleophiles, Organometallics, 1989, 8, 521-529.

49 V. G. Albano, S. Bordoni, L. Busetto, A. Palazzi, P. Sabatino, V. Zanotti, Dithiocarbamate derivatives of μ-hiocarbyne complexes: synthesis and X-ray molecular structure of $[Fe_2(\mu\text{-}CS)(\mu\text{-}CSMe)(\mu\text{-}S_2CNMe_2)Cp_2]$, J. Organomet. Chem. 2002, 659, 15-21.

50 N. C. Schroeder, Reactivity of bridging thiocarbyne complexes of iron, Ph.D. Dissertation, Iowa State University, Ames, IA, 1985, https://lib.dr.iastate.edu/rtd/7884

51 According to Cahn–Ingold–Prelog priority rules, the E isomer of $[\mathbf{3}]^+$ features the SMe group on the same side of the carbonyl ligand.

52 V. G. Albano, S. Bordoni, L. Busetto, M. Monari, V. Zanotti, An Unusual Hydrogen Migration from a Cyclopentadienyl to a μ-Carbyne Carbon in the Reaction of Grignard Reagents with $[Fe_2(CO)_2(cp)_2(\mu\text{-}CO)(\mu\text{-}CSMe)]SO_3CF_3$, Organometallics 1995, 14, 5455-5457.

53 L. S. Lazarus, A. D. Benninghoff, L. M. Berreau, Development of triggerable, trackable, and targetable carbon monoxide releasing molecules, Acc. Chem. Res. 2020, 53, 2273-2285.

54 K. Ling, F. Men, W.-C. Wang, Y.-Q. Zhou, H.-W. Zhang, D.-W. Ye, Carbon monoxide and its controlled release: therapeutic application, detection, and development of carbon monoxide releasing molecules (CORMs) miniperspective, J. Med. Chem. 2018, 61, 2611-2635.

55 A. De Palo, D. Draca, M. G. Murrali, S. Zacchini, G. Pampaloni, S. Mijatovic, D. Maksimovic-Ivanic, F. Marchetti, A Comparative Analysis of the In Vitro Anticancer Activity of Iridium(III) $\{\eta^5\text{-}C_5Me_4R\}$ Complexes with Variable R Groups, Int. J. Mol. Sci. 2021, 22, 7422.

56 D. Rocco, L. K. Batchelor, G. Agonigi, S. Braccini, F. Chiellini, S. Schoch, T. Biver, T.Funaioli, S. Zacchini, L. Biancalana, M. Ruggeri, G. Pampaloni, P. J. Dyson, F. Marchetti, Anticancer potential of diiron vinyliminium complexes, Chem. Eur. J. 2019, 25, 14801-14816.

57 O. A. Lenis-Rojas, M. P. Robalo, A. I. Tomaz, A. Carvalho, A. R. Fernandes, F. Marques, M. Folgueira, J. Y. Çez, D. Vazquez-Garcia, M. Ljpez, Torres, A. Fernandez, J. J. Fernandez, Ru^{II}(p-cymene) Compounds as Effective and Selective Anticancer Candidates with No Toxicity in Vivo, Inorg. Chem. 2018, 57, 13150–13166.

58 O. Zilka, R. Shah, B. Li, J. P. Friedmann Angeli, M. Griesser, M. Conrad, D. A. Pratt, On the Mechanism of Cytoprotection by Ferrostatin-1 and Liproxstatin-1 and the Role of Lipid Peroxidation in Ferroptotic Cell Death, ACS Cent. Sci. 2017, 3, 232−243.

59 H. Adibi, S. Abdolmaleki, N. Shahabadi, A. Golabi, M. Mahdavi, S. Zendehcheshm, M. Ghadermazi, M. Ansari, H. A. Rudbari, G. Bruno, A. Nemati, Investigation of crystallographic structure, in vitro cytotoxicity and DNA interaction of two La(III) and Ce(IV) complexes containing dipicolinic acid and 4-dimethylaminopyridine, Polyhedron 2019, 163, 20-32.

60 T. C. Bernardo, T. Cunha-Oliveira, T. L. Serafim, J. Holy, D. Krasutsky, O. Kolomitsyna, P. Krasutsky, A. M. Moreno, P. J. Oliveira, Dimethylaminopyridine derivatives of lupane triterpenoids cause mitochondrial disruption and induce the permeability transition, Bioorg. Med. Chem. 2013, 21, 7239-7249.

61 I. Kaljurand, A. Kutt, L. Soovali, T. Rodima, V. Maemets, I. Leito, I. A. Koppel, Extension of the Self-Consistent Spectrophotometric Basicity scale in Acetonitrile to a Full Span of 28 pKa Units: Unification of Different Basicity Scales, J. Org. Chem. 2005, 70, 1019-1028

62 H. Feng, B. R. Stockwell, Unsolved mysteries: How does lipid peroxidation cause ferroptosis?, PLoS Biol. 2018, 16, e2006203.

63 K. Subburayan, F. Thayyullathil, S. Pallichankandy, A. Rahman Cheratta, S. Galadari, Superoxide-mediated ferroptosis in human cancer cells induced by sodium selenite, Transl. Oncol. 2020, 13, 100843.

64 J. Zhou, Y. Pang, W. Zhang, F. OuYang, H. Lin, X. Li, J. Yan, Discovery of a novel stilbene derivative as a microtubule targeting agent capable of inducing cell ferroptosis, J. Med. Chem. 2022, 65, 4687–4708.

65 T. Homma, S. Kobayashi, M. Conrad, H. Konno, C. Yokohama, J. Fujii, Nitric Oxide 2021, 115, 34-43.

66 E. Castro-Pérez, M. Singh, S. Sadangi, C. Mela-Sánchez, V. Setaluri, Connecting the dots: Melanoma cell of origin, tumor cell plasticity, trans-differentiation, and drug resistance, Pigment Cell Melanoma Res. 2023, 36 330-347.

67 S. Mijatović, A. Bramanti, F. Nicoletti, P. Fagone, G. N Kaluđerović, D. Maksimović-Ivanić, Naturally occurring compounds in differentiation based therapy of cancer, Biotechnol. Adv. 2018, 36, 1622-1632.

68 D. Maksimovic-Ivanic, S. Mijatovic, D. Miljkovic, L. Harhaji-Trajkovic, G: Timotijevic, M. Mojic, D. Dabideen, K. F. Cheng, J. A. McCubrey, K. Mangano, Y. Al-Abed, M. Libra, G: Garotta, S. Stosic-Grujicic, F. Nicoletti, The antitumor properties of a nontoxic, nitric oxide–modified version of saquinavir are independent of Akt, Mol. Cancer Ther. 2009, 8, 1169-1178.

69 S.G. Slutsky, A. K. Kamaraju, A. M. Levy, J. Clebath, M. Revel, Activation of myelin genes during transdifferentiation from melanoma to glial cell phenotype, J. Biol. Chem. 2003, 278, 8960–8968.

70 S. S. Brar, T.P. Kennedy, A.B. Sturrock, T.P. Huecksteadt, M.T. Quinn, A. R. Whorton, J. R. Hoidal, An NAD(P)H oxidase regulates growth and transcription in melanoma cells, Am. J. Physiol.-Cell. Ph. 2002, 282, C1212-C1224.

71 S. Koga, M. Nakano, S. Tero-Kubota, Generation of superoxide during the enzymatic action of tyrosinase, Arch. Biochem Biophys. 1992, 292, 570-575.

72 R. E. Wagner, R. A. Jacobson, R. J. Angelici and M. H. Quick, Synthesis of thiocarbonyl-bridged (η^5-$C_5H_5)_2Fe_2(CO)_3(CS)$ and crystal structure of an S-alkylated derivative, J. Organomet. Chem. 1978, 148, C35-C39.

73 M. H. Quick, R. J. Angelici, Synthesis and cleavage reactions of thiocarbonyl-bridged $Cp_2Fe_2(CO)_3CS$, and preparation of the carbene complexes $CpFe(CO)C(N_2C_2H_6)SnPh_3$ and $[CpFe(CO)_2C(OMe)_2]PF_6$, J. Organomet. Chem. 1978, 160, 231-239.

74 B. D. Dombek, M.-G. Choi, R. J. Angelici, I. S. Butler, D. Cozak, Dicarbonyl(η^5-Cyclopentadienyl)-(Thiocarbonyl)Iron(1+) Trifluoromethane-Sulfonate(1–) and Dicarbonyl(η^5-Cyclo-Pentadienyl)[(Methylthio)Thiocarbonyl]Iron, Inorg. Synth. 1990, 28, 186-189.

75 G. R. Fulmer, A. J. M. Miller, N. H. Sherden, H. E. Gottlieb, A. Nudelman, B. M. Stoltz, J. E. Bercaw and K. I. Goldberg, NMR Chemical Shifts of Trace Impurities: Common Laboratory Solvents, Organics, and Gases in Deuterated Solvents Relevant to the Organometallic Chemist, Organometallics 2010, 29, 2176-2179.

76 R. K. Harris, E. D. Becker, S. M. Cabral De Menezes, R. Goodfellow and P. Granger, NMR nomenclature. Nuclear spin properties and conventions for chemical shifts (IUPAC Recommendations 2001), Pure Appl. Chem. 2001, 73, 1795-1818.

77 F. Menges, "Spectragryph - optical spectroscopy software", Version 1.2.16.1, @ 2016-2022, http://www.effemm2.de/spectragryph.

78 R. J. Hewitt, M. Jui Hsien Ong, Y. Wee Lim and B. A. Burkett, Investigations of the Thermal Responsiveness of 1, 4, 2-Oxathiazoles, Eur J. Org. Chem. 2015, 30, 6687-6700.

79 A. K. Mailyan, J. L. Chen, W. Li, A. A. Keller, S. M. Sternisha, B. G. Miller and A. Zakarian, Short Total Synthesis of $[^{15}N_5]$-Cylindrospermopsins from $^{15}NH_4Cl$ Enables Precise

Quantification of Freshwater Cyanobacterial Contamination, J. Am. Chem. Soc. 2018, 140, 6027-6032.

80 S. Sato, N. Furukawa, Sci. Synth. 2005, 18, 821-968.

81 The $CF_3SO_3^-$ salt was first mentioned in: L. Busetto, S. Bordoni, V. Zanotti, V. G. Albano, D. Braga, Gazz. Chim. Ital. 1988, 118, 667.

82 G. M. Sheldrick, SADABS-2008/1 - Bruker AXS Area Detector Scaling and Absorption Correction, Bruker AXS: Madison, Wisconsin, USA, 2008.

83 G. M. Sheldrick, Crystal structure refinement with SHELXL, Acta Cryst. C, 2015, 71, 3-8.